Chapter 10

Organic Semiconductors for Non-Linear Optical Applications

Anca Stanculescu and Florin Stanculescu

Additional information is available at the end of the chapter

http://dx.doi.org/10.5772/60926

Abstract

The organic molecules represent a promising research field because they show special properties which are determined by the conjugated system of π electrons and the groups substituted to the aromatic nucleus offering perspectives for a large area of applications, including the non-linear optics.

We have investigated two types of molecular crystalline material prepared from aromatic derivatives, meta-dinitrobenzene (m-DNB) and benzil (Bz), and three types of organic thin films prepared from arylenevinylene (triphenylamine, carbazole) compounds, maleimidic derivatives and anilinic derivatives functionalised copolymers using different methods (matrix-assisted pulsed laser evaporation, vacuum evaporation, spin coating). The effect of the experimental conditions on the morphological and structural particularities of the films has been emphasised. New results are bought about the systems formed from an aromatic derivative (m-DNB and benzil) crystal and inorganic (organic) dopant studied from the point of view of the dopant incorporation considering the stability of the growth interface and its effect on the optical band gap and optical non-linear (ONL) properties of the m-DNB and Bz crystals. The relationship between the morphology and structural order of the maleimidic derivatives monomers in polycarbonate matrix composite layer and the ONL properties is discussed. We analysed the correlation between the molecular structure of organic compound, particularities of the macroscopic order (influenced by the crystal growth and thin-film deposition methods) and optical non-linear (second harmonic generation, two-photon fluorescence) properties.

Keywords: Organic materials, optical non-linear properties, thin films, organic crystals

1. Introduction

The past decades indicated a large-scale development of the optical telecommunications conditioned by the improvement of the optical fibres performances. The research activity in the field of non-conventional optical effects in a variety of materials has been stimulated by the discovery of the laser emission. The information transmission velocity using light determines an increase in the efficiency of the systems used in a large area of applications from communications to medicine and military domain as well as a direct control at the optical signal level, without the necessity of an optical-electronic-optical conversion. The examples include the liquid crystals for displayers, piezoelectric plastic materials for microphones, active organic materials for luminescent displayers (OLED), as well as the organic materials with special optical properties in solid state for applications in photonics. The optical non-linear materials are assumed as the key elements for further photonic applications, because these allow the control on the luminous beam using another luminous beam.

The exploitation of the remarkable properties of the organic molecules represents a new and promising technological field, because the specific properties of the molecular structure determines the response (selective, fast, intense) at macroscopic level, under some external stimulus action, like luminous radiation. The organic compounds are intensively studied because they show special properties which are associated with the conjugated system of π electrons and the groups substituted to the aromatic nucleus generating intra-molecular charge transfer properties associated with a large area of applications, including the non-linear optics and offering an alternative to the inorganic compounds.

In the field of optical non-linear (ONL) applications, the interest is correlated with the preparation of crystals and thin films from molecular, oligomeric and polymeric materials with conjugated systems, extended π electrons systems and active optical non-linear chromophoric groups, showing an arrangement of the chromophores adequate for the appearance of some favourable physical properties. The high non-linearity of (molecular and oligomeric/polymeric) organic materials is due to the large delocalisation of π electrons cloud, which can be determined by the electronegativity of the functional groups, chromophores, substituted to the aromatic nucleus and operating as electron donors or acceptors. Supplementary, in order to generate optical non-linear effects, it is necessary to pack the organic molecules in a non-symmetrical macroscopic form. These conditions could be satisfied in bulk molecular crystal or in polymers/monomers thin-films materials because they are characterised by a high molecular order and density of chromophoric groups. In the case of molecular crystals special requirements concern the crystallinity, and in the case of monomers and polymeric materials special requirements concern the quality of the thin films. The main characteristics making favourable the utilisation of the organic molecular crystals for the mentioned applications are: large transparency domain, high birefringency, high non-linear coefficients, high damage thresholds in laser beam, versatility of the molecular structure which can be changed by molecular engineering for optimising the properties of interest [1, 2]. Since the discovery of the high optical non-linearities of the organic materials, the interest for these materials considerably grew up, opening new directions for studying and identifying new applications in the photonics field.

http://dx.doi.org/10.5772/60926

Lately, there is significant growth of the interest in analysing the potential of organic materials for new applications in the dynamic processing of image implying: optical conversion of frequency [3]; electro-optical modulation [4]; dynamic holography [5]; real-time interferometry [6]; optical storage of information; optical conjugation of phase [7]; optical amplification of image [8]; spatial modulation of the light [9]; optical interconnection [10]. Organic materials can be also utilised in the field of second harmonic generation (SHG) for medical applications and two-photon fluorescence (TPF) for biological imaging microscopy [11, 12].

In the field of non-linear optics, the two photons absorption (TPA) is a third-order process correlated with the extended π-conjugated electronic structures and charge transfer properties, which can be indirectly evaluated by two photons absorption emission fluorescence (TPF). Organic compounds showing TPA are interesting for potential applications in frequency up conversion lasing, optical power limiting, 3D fluorescence imaging, 3D optical data storage, 3D lithographic microfabrication and photodynamic therapy [13-15].

There is a tight bond between the material properties and the preparation conditions (synthesis, crystal growth and films deposition) just like between the molecular structure and the properties of interest. The properties of these materials are strongly affected by the presence of structural and/or chemical defects. Therefore, the special promises associated with the potential performances of these materials related to intrinsic properties of material could be valorised only solving the concrete problems involved by the manufacture of a material having the desired form, dimension, quality and properties adequate for a target application. For this reason of great importance is the identification of the optimal methods to prepare these materials both in crystalline form (molecular organic compounds) and as thin films (monomeric/polymeric compounds). In this context, a special attention must be paid to the design, synthesis and characterization of the organic compound, preparation and evaluation of the optical non-linear properties of the organic material for photonic/optoelectronic applications. Till now, a satisfactory compromise between the theoretically predicted non-linearity and the quality of the materials related to preparation and processing challenges has not been obtained for organic materials.

The purpose of this chapter is to enlarge the knowledge about the optical properties and processes involved in the interaction of light with the organic solid state showing new molecular structures and about the correlation between the preparation conditions of the molecular/oligomeric/polymeric materials and their physical characteristics. This will offer a way to restrain the organic compounds by selecting the adequate materials for target photonic applications focusing on non-linear optics. The correlation between the molecular structure of monomer, oligomer and polymer, type of macroscopic order (associated with the growth method for crystal and deposition method for thin film) and optical non-linear (SHG, TPF) properties (involving interaction phenomena of radiation with organic compounds) will be emphasised.

2. Bulk organic semiconductors for optical non-linear applications

The aromatic derivatives such as meta-dinitrobenzene (m-DNB) and benzil (Bz) are organic compounds of interest in preparing bulk crystal materials showing large transparency domain,

large optical band gap and high non-linear coefficients. These two compounds show important optical non-linear phenomena despite the differences in their chemical structure at the molecular level. In the context of special attention paid to the investigation of bi-component organic systems for optical non-linear (ONL) applications involving the synthesis of the organic compounds, organic crystal growth and characterisation, the interest in studying m-DNB and Bz bulk crystals is justified by the perspective to use these materials as a crystalline host matrix for both organic and inorganic guests.

m-DNB ($C_6H_4N_2O_4$) is a negative bi-axial crystal that belongs to the Pbn21 space group and the point symmetry group mm2 which crystallises in the orthorhombic system at room temperature showing a pyramidal shape. The unit cell contains four molecules and has the following dimensions: a = 13.20 Å, b = 13.97 Å and c = 3.80 Å. The transparency range of m-DNB crystalline materials is 0.4-2.5 μm [16, 17, 19]. Bz ($C_6H_5COCOC_6H_5$) is an uni-axial crystal that belongs to the trigonal space group $P3_12_1$ and the point symmetry group $D_3^4\left(D_3^6\right)$. The unit cell contains three molecules which are helically disposed and closely packed around the 31 axis and the hexagonal unit cell has the following dimensions: a = 8.42 Å and b = 13.75 Å. The transparency range of Bz crystalline materials is from UV through near IR [18, 19].

Pure m-DNB and Bz crystals have been grown from the melt by the Bridgman-Stockbarger method using the same experimental set-up and the same experimental conditions defined by a temperature gradient (ΔT) of 25°C cm^{-1} and growth speed (v) of 1.7 mm h^{-1} [19]. The crystal of m-DNB doped with iodine has also been grown in the same experimental set-up and the same experimental conditions such as the crystal of Bz doped with iodine or m-DNB: ΔT = 30°C cm^{-1} and v = 2.0 mm h^{-1} [19].

We have developed some studies about the influence of the crystal growth conditions on the incorporation of dopant and the effect of dopant on the optical properties of pure m-DNB and Bz crystals. We have analysed the two aromatic derivatives crystals from two different perspectives: (1) the effect of iodine (I_2) dopant concentration (1 wt% and 2 wt%) on the two different matrix (m-DNB and Bz) and (2) the behaviour of the same aromatic derivative, m-DNB, as matrix and dopant [19].

The X-ray diffraction study of pure and doped m-DNB and Bz crystals has offered data which have been analysed in the Pawley approach with the TOPAS software emphasising the effect of dopant on the lattice parameters [19].

The study has been realised on slices cut perpendicularly to the growth direction of the crystal. The sharp diffraction peaks shown in Figure 1 sustain a good crystallinity of the bulk materials and these peaks have been attributed using the Power Diffraction File for m-DNB and Bz which contains the reference values of the lattice parameters. The crystallographic planes which give the strongest reflections are parallel to the surface of the slice and therefore, the strongest reflection is given in Bz by the (003) plane, the growth direction of the crystal being [001] and the strongest reflections in m-DNB are given by the (111), (311) and (002) planes confirming the polycrystalline nature of the grown crystal showing three regions of three different orientations [19].

http://dx.doi.org/10.5772/60926

The values of lattice parameters obtained for the hexagonal benzil crystal, $a = b = 8.350$ Å and $c = 13.557$ Å, are in agreement with the reference value, $a = b = 8.410$ Å and $c = 13.679$ Å [19]. The lattice parameters evaluated for m-DNB orthorhombic crystal, $a = 13.246$ Å, $b = 14.029$ Å and $c = 3.807$ Å, are also in agreement with the reference values, $a = 13.290$ Å, $b = 14.070$ Å and $c = 3.813$ Å [19]. The slight smaller experimental values of a and b compared to the reference values suggest a compression of the lattice and the presence of some internal stress/strain. Considering the effect of dopant on the lattice parameter of the matrix, we can obtain information on the type of mechanism which could be involved in the incorporation of dopant: in interstitial or in substitutional positions. By doping with I_2 the lattice parameters of Bz have increased from $a = b = 8.350$ Å to $a = b = 8.453$ Å and from $c = 13.557$ Å to $c = 13.622$ Å. These values confirm an interstitial incorporation of I_2 dopant in Bz matrix [19]. A similar behaviour and interstitial incorporation is also shown by I_2 in m-DNB matrix, the lattice parameters of pure m-DNB increasing by doping with I_2 from $a = 13.246$ Å to $a = 13.345$ Å, from $b = 14.029$ Å to $b = 14.186$ Å and from $c = 3.807$ Å to $c = 3.821$ Å [19].

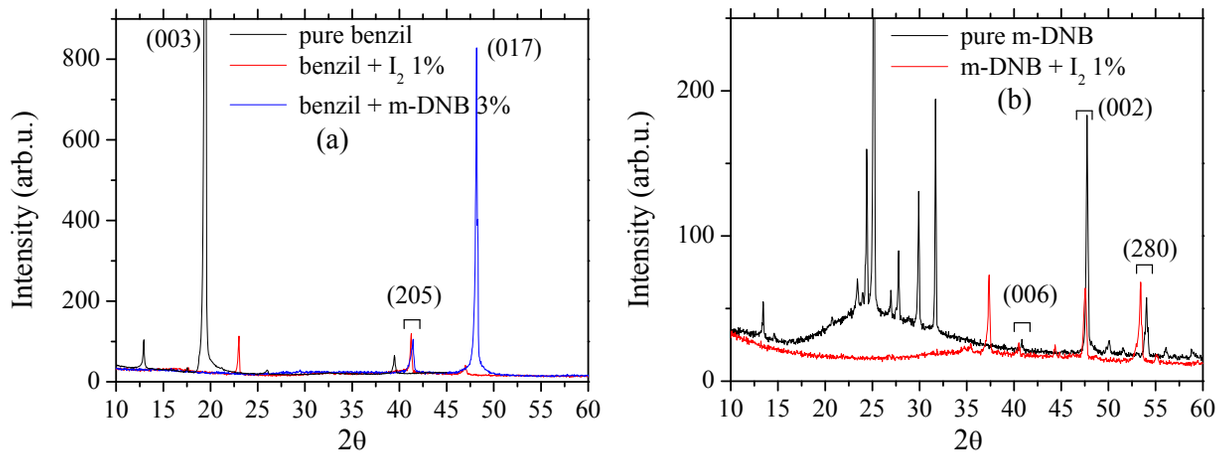

1

Figure 1. XRD patterns for pure and doped Bz (a) and pure and doped m-DNB (b) [19].

On the contrary, by doping with m-DNB the Bz crystal lattice parameters a and b have decreased from $a = b = 8.350$ Å to $a = b = 8.267$ [19] confirming a substitutional incorporation of m-DNB molecule in Bz, the molecule of m-DNB being smaller than the molecule of benzil.

The optical properties of the organic crystal are affected by the quality of the crystal determined by the shape of the solid-liquid interface through the growth conditions. Additionally, the homogeneity is very important for the doped crystals and is directly connected to the dopant incorporation determined also by the solid-liquid interface shape.

In this context, new results have been bought about the systems aromatic derivative/dopant studied from the point of view of the growth interface stability criterion represented by eq. (1) with the purpose to analyse the incorporation of dopant and its effect on the quality of the crystal. The stable growth limits and the experimental conditions related to temperature gradient at the growth interface and moving speed of the ampoule in the furnace have been investigated.

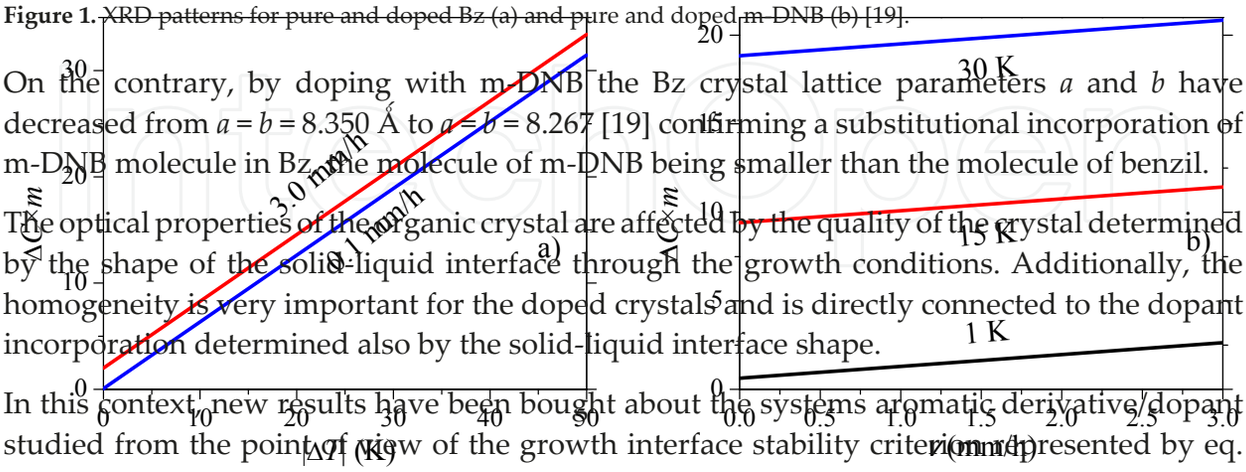

2

The previous results on growth interface stability for Bz crystal [20, 21] have been completed with new conclusions on the stable growth of m-DNB crystals. We will emphasise the conditions favouring the initiation of instabilities, which are associated with structural defects and compositional non-homogeneities in the crystal of m-DNB affecting the optical properties including the ONL properties.

A slightly convex liquid-solid interface is necessary to obtain good-quality crystals, but during the growth process the shape of the interface changes as a consequence of the variation in the thermal conductivity of the organic compound in the liquid and solid state. Because the ratio between the thermal conductivity coefficient in melt and solid is ≤1 both for m-DNB and Bz, it is predicted a convex growth interface with a lower deviation from the planar growth interface in the case of Bz. This conclusion confirms that it is easier to grow good-quality Bz than m-DNB crystals [19].

The stability of the growth interface in the binary system m-DNB doped with iodine has been considered as an example for analysing the solidification process in doped m-DNB crystals [22-24]. Starting with the stability criterion we have drawn the curves $\Delta C \times \cdot m = f(\Delta T)$ at v = const. and $\Delta C \times m = f(v)$ at ΔT=const, where

$$\Delta C \cdot m \le \frac{\rho_m \cdot \Delta_f H}{k_m + k_s} \cdot v - \frac{2 \cdot k_m}{k_m + k_s} \cdot \Delta T \tag{1}$$

and ΔT = thermal gradient at the growth interface; ΔC = gradient of concentration in the liquid at the growth interface; m = liquidus line slope; v = moving speed of the interface during the solidification process; ρ_m = melt density; $\Delta_f H$ = enthalpy of fusion; k_s = thermal conductivity of the solid; k_m = thermal conductivity of the melt. For m-DNB we have used the following values for constants [19]: $\Delta_f H$ = 17.30 kJ mol^{-1} [25], ρ_m = 1.3644 g cm^{-3} [26], k_m = 0.183×10^{-2} Wcm^{-1}K^{-1} [27] and k_s = 0.4×10^{-2} W cm^{-1}K^{-1} [28].

In the Bridgman-Stockbarger configuration, above these curves presented in Figure 2, it is situated the region of stable growth and below, the region of unstable growth. For the curves corresponding to $\Delta C \times \cdot m = f(\Delta T)$ at v = const. shown in Figure 2a and high concentration gradients at the interface, the stable growth can not be assured at low-temperature gradients even for high moving speed. For the curves corresponding to $\Delta C \times m = f(v)$ at ΔT = const. shown in Figure 2b, the area of the stable growth region increases with the increase in thermal gradient, the increase in the interface moving velocity being not critical [19]. Therefore, to be situated in the stable growth region for high values of the product $\Delta C \times m$, we have to assure high thermal gradient by adequately positioning the ampoule in the thermal profile of the heater.

As a consequence, the experimental conditions used to grow pure m-DNB crystals (ΔT = 25°C, v = 1.7 mm h^{-1}) and iodine doped m-DNB crystals (ΔT = 30°C, v = 2.0 mm h^{-1}) are fixing the limits for the product $\Delta C \times m$ that assure a stable growth and are compatible with the experimental conditions for a stable growth of pure and doped benzil crystals, previously presented [20, 21]. Therefore, it is possible to grow m-DNB and Bz crystals in the same experimental

http://dx.doi.org/10.5772/60926

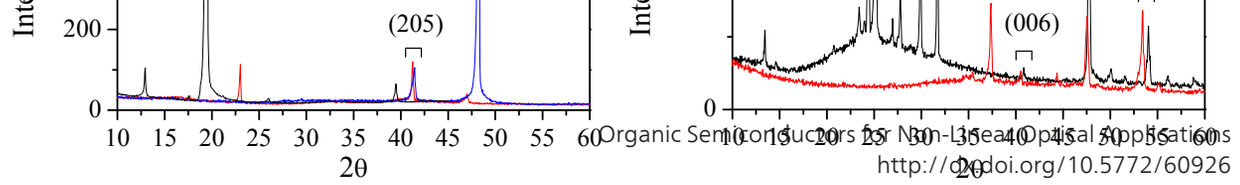

1

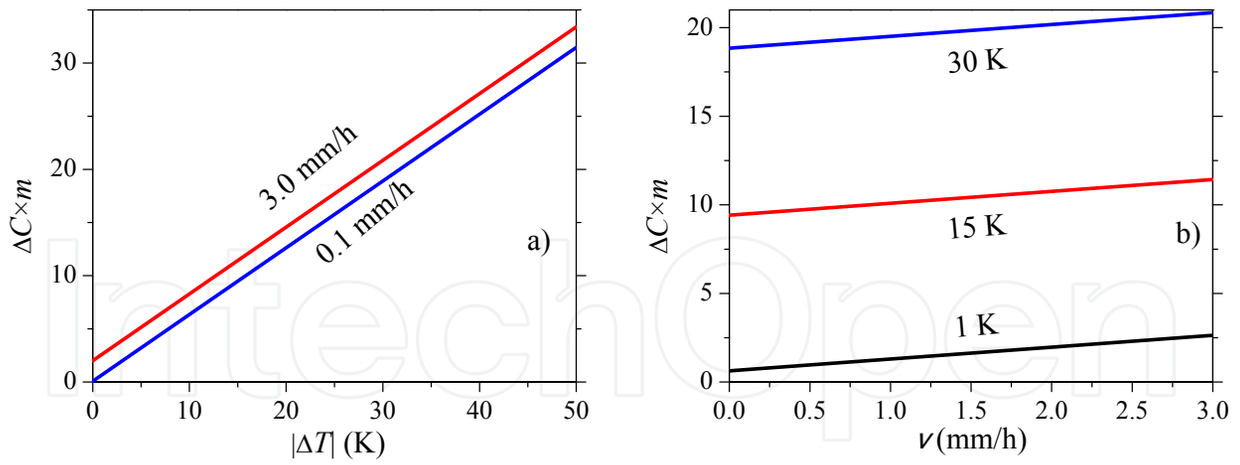

2

Figure 2. Stable and unstable growth region for m-DNB: $\Delta C \times m = f(v)$ at ΔT = const. (a); $\Delta C \times \cdot m = f(\Delta T)$ at v = const. (b) [19].

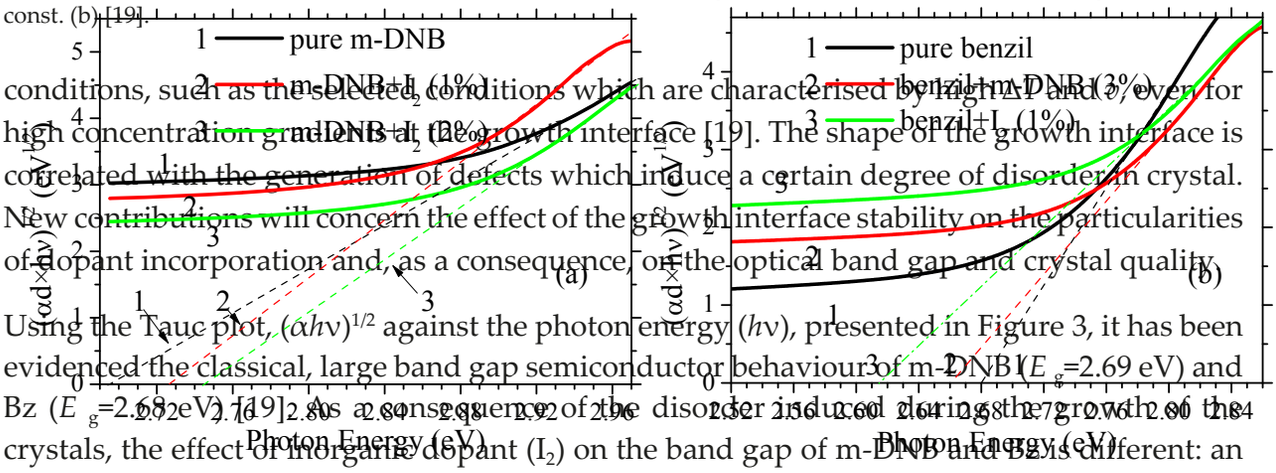

3

conditions, such as the selected conditions which are characterised by high ΔT and v, even for high concentration gradients at the growth interface [19]. The shape of the growth interface is correlated with the generation of defects which induce a certain degree of disorder in crystal. New contributions will concern the effect of the growth interface stability on the particularities of dopant incorporation and, as a consequence, on the optical band gap and crystal quality.

Using the Tauc plot, $(\alpha h\nu)^{1/2}$ against the photon energy ($h\nu$), presented in Figure 3, it has been evidenced the classical, large band gap semiconductor behaviour of m-DNB (E_g=2.69 eV) and Bz (E_g=2.68 eV) [19]. As a consequence of the disorder induced during the growth of the crystals, the effect of inorganic dopant (I_2) on the band gap of m-DNB and Bz is different: an increase in m-DNB band gap, tendency maintained with increasing iodine concentration and a decrease in Bz band gap, tendency maintained also for organic dopants (m-DNB).

The m-DNB crystals have shown a higher disorder (evidence by Urbach law) compared to benzil crystal grown in the same experimental conditions [19]. The Urbach energy has been evaluated from the slope of the plot ($\ln\alpha$) against ($h\nu$) in the region of low energy. The m-DNB crystals doped with I_2 have shown a lower disorder than the undoped crystals. While I_2 dopant increases the degree of disorder in Bz crystal, the effect of organic dopant (m-DNB) is, on the contrary, smaller [19].

A special configuration presented in Figure 4 has been used for the excitation of ONL phenomena in organic materials samples both bulk crystals (mentioned above) and thin films (will be introduced later). The experimental set-up is based on an ultra short pulsed laser Spectra Physics 'Tsunami' characterised by a maximum wavelength of 800 nm, pulse duration of 60 fs, frequency of 80 MHz and medium power of 780 mW [29].

A high N.A. Mitutoyo microscope objective was used to focus the laser beam on the sample mounted on a motorised Thorlabs XYZ stage. The same microscope objective used for irradiation is also used for collecting the light emitted by the sample in 180 degrees geometry.

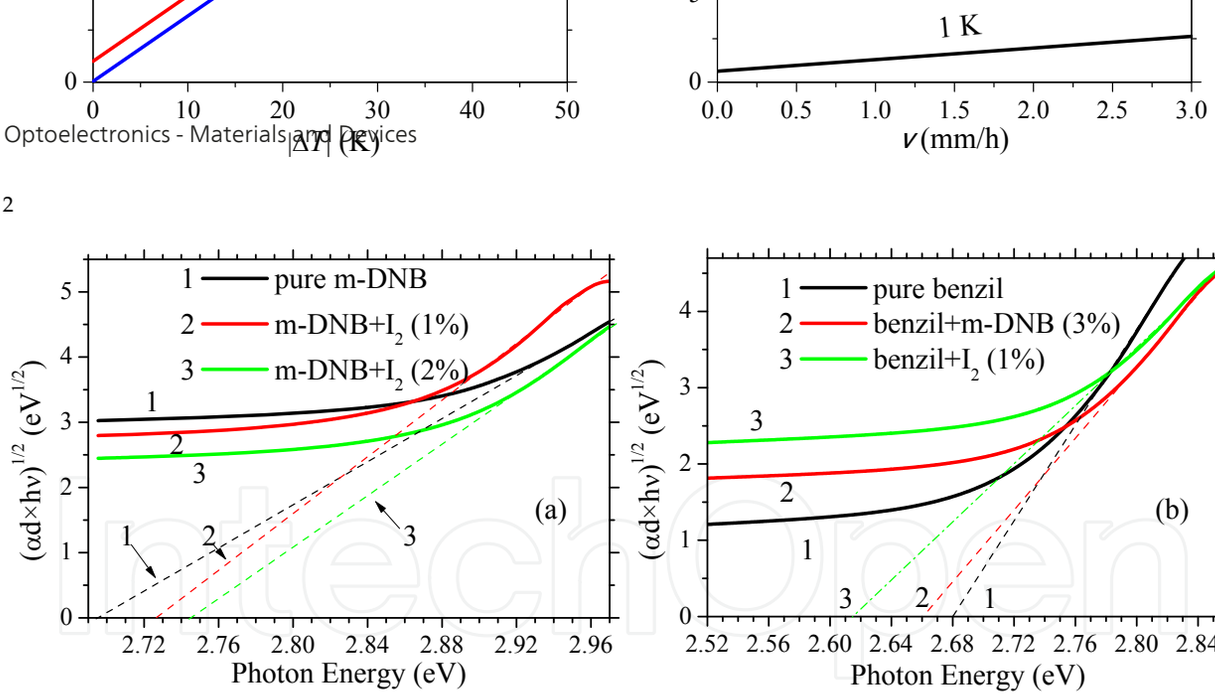

Figure 3. Tauc plots for: pure and doped m-DNB (a); pure and doped Bz (b) [19].

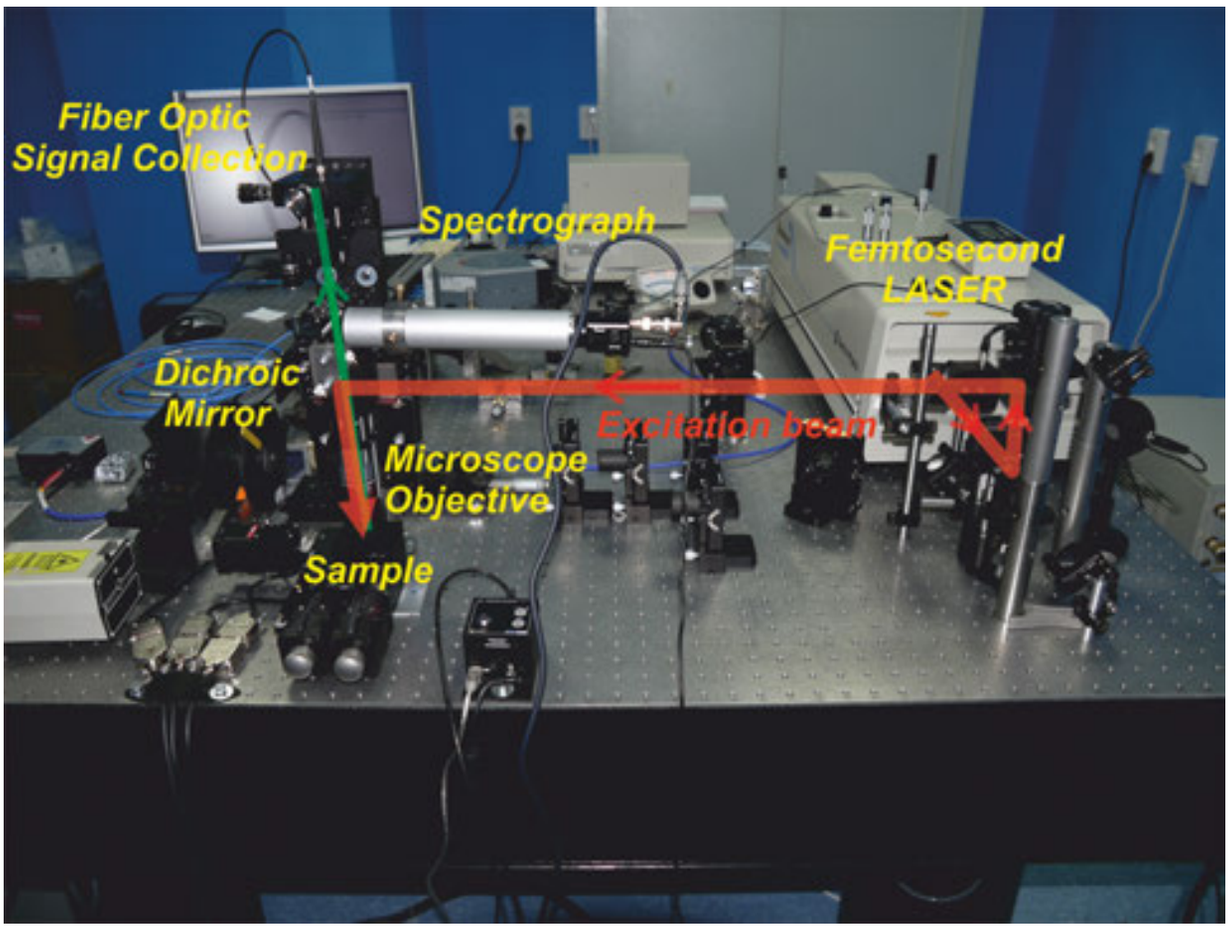

Figure 4. Experimental set-up for ONL phenomena measurements.

The detection system is optimised to be sensible in the visible range. The emitted light is passing through a dichroic mirror and, after this, is focused by a lens on the collecting optical fiber connected with a spectrograph ANDOR Shamrock 163i. An ANDOR IDUS CCD camera

http://dx.doi.org/10.5772/60926

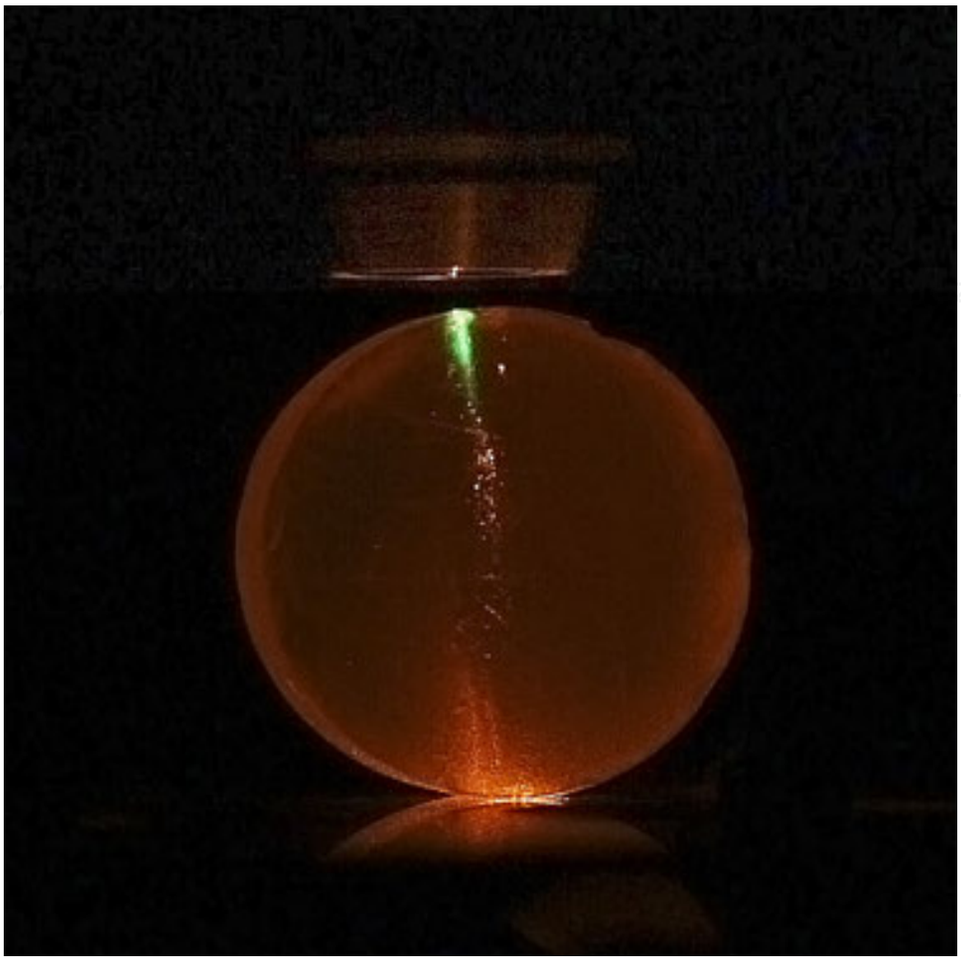

Figure 5. Image of the ONL signals obtained in a crystal of Bz.

cooled at 213 K is used to measure the dispersed light. The excitation light is blocked and its effect is minimised with a NIR cut-off filter placed in front of the focalisation lens. The amplification of the CCD detector can be increased without the necessity to increase the signal at longer wavelengths [29].

The intensity of optical non-linear phenomena, like SHG and TPF, associated to green light in Figure 5, produced in aromatic derivative crystals is also affected by the stability of the growth interface and the presence of defects.

The two types of aromatic derivatives crystals grown in the same experimental conditions show different dominant ONL phenomenon. In m-DNB, SHG dominates while in Bz, TPF dominates as can be seen in Figure 6.

In two-photon absorption process (TPA) two photons combine to bridge a gap of energy larger than the energy corresponding to each individual photon. This process is not involving any intermediate or virtual state created by the interaction of the photons with the organic molecules, the two photon absorption emission fluorescence (TPF) being an indirect measure of this process.

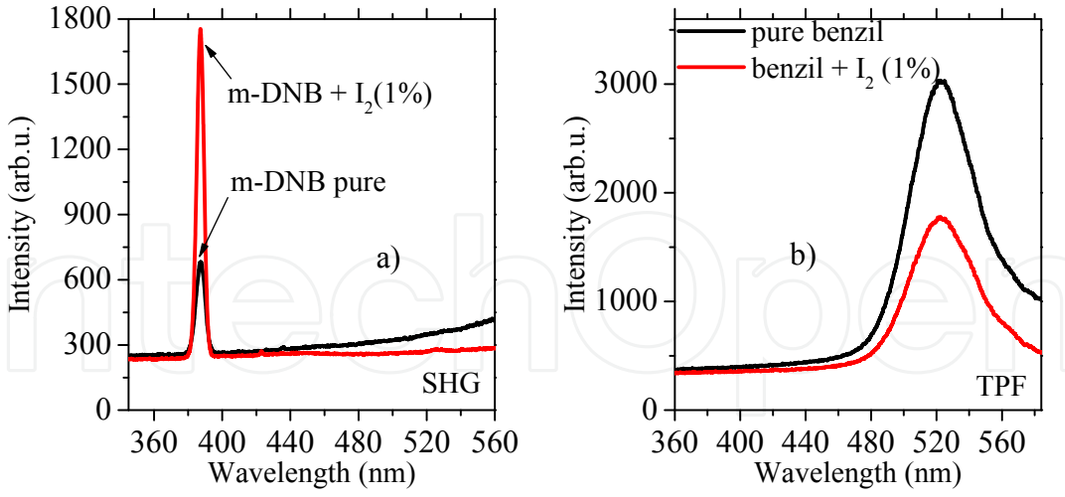

Figure 6. ONL phenomena in organic molecular crystalline materials: m-DNB (a); Bz (b) [19].

The SH associated with the peak situated around 400 nm is determined in m-DNB by the inductive and mezomeric effects associated with the strongly polarisable substituent groups of -NO_2. The ONL phenomena in Bz are determined by the long conjugated chain causing a displacement of the charge inside the delocalised π-electrons over two aromatic rings and two carbonyl groups. The broad emission band centred around 540 nm is determined by the luminescence obtained by two-photon absorption because Bz has an electronic excited level corresponding to singlet excited state (n, π*) in skew configuration situated at 3.2 eV [30]. This energy is close to that corresponding to a photon with twice the frequency of the laser beam and generates the excitation at the edge of the absorption band. After excitation, the relaxation of the Bz lattice implies three steps: (1) the planar rearrangement of molecules and redistribution of energy, because the carbonyl groups emit only from the planar configuration characterised by an energy level situated at 2.6 eV; (2) radiationless relaxation by a process of intersystem crossing to the first triplet excited state situated at 2.3 eV; (3) radiative de-excitation generating the emission band centred on 540 nm, the position and shape of this band corresponding to the usual fluorescence in Bz at linear excitation [19].

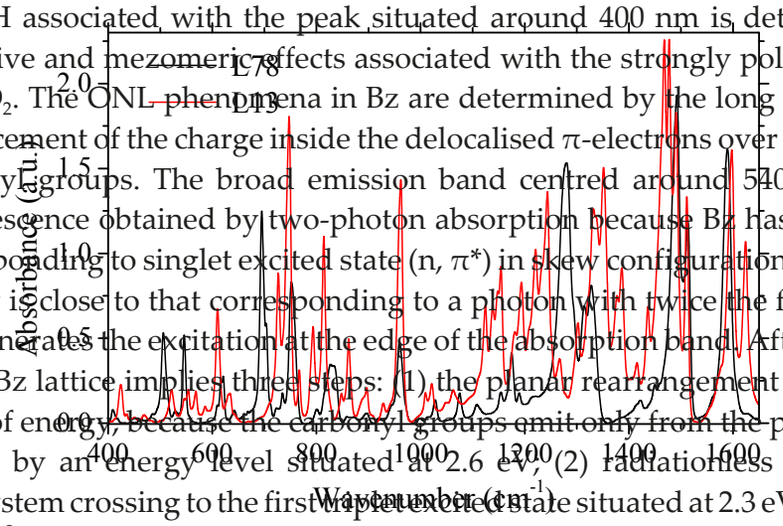

The intensity of SH signal increases in m-DNB doped with I_2 compared to pure m-DNB, in concordance with the lower degree of disorder associated with lower Urbach energy in the grown doped crystal. ONL properties are enhanced by the deformation of the m-DNB molecule in the presence of I_2 determining an asymmetry in the electronic cloud. The intensity of TPF signal decreases in Bz crystals doped with I_2 grown in the same experimental conditions as a consequence of the increased disorder associated with higher Urbach energy favouring absorption/scattering of radiation.

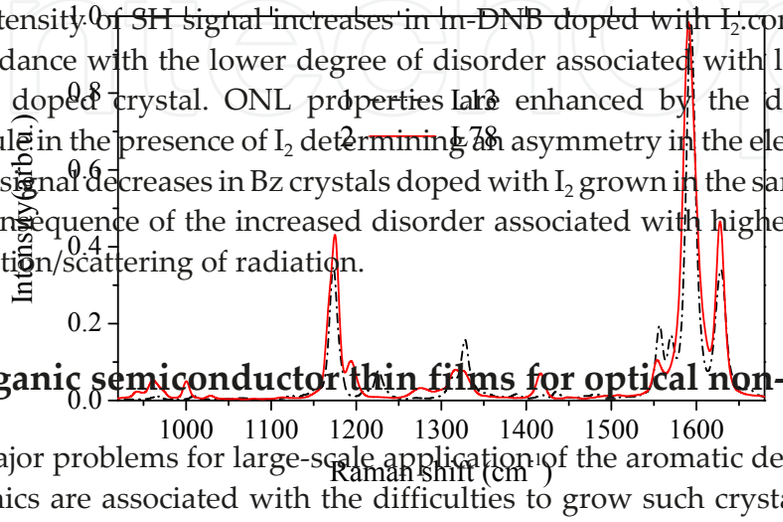

3. Organic semiconductor thin films for optical non-linear applications

The major problems for large-scale application of the aromatic derivatives as bulk crystals in photonics are associated with the difficulties to grow such crystals (determined by the low

melting point, supercooling, low thermal conductivity) and to process the crystals (determined by the low mechanical properties imposed by the weak bonding forces between molecules). Other difficulty is related to the homogeneous distribution of the dopant within the matrix. Therefore, the thin films are preferred, but the same problems correlated with the properties of the organic compounds still remain and involve adequate method for thin-films preparation, like vacuum evaporation deposition, matrix-assisted pulsed laser evaporation (MAPLE) and spin coating, in correlation with the particularities of the organic molecule. We have selected and investigated three types of organic thin films prepared from arylenevinylene compounds, maleimidic derivatives and anilinic derivatives functionalised copolymers.

3.1. Thin films based on arylenevinylene compounds

From arylenevinylene compounds we have selected triphenylamine- and carbazole-based compounds whose chemical structures are presented in Figure 7, two aromatic amines, which could be used as building blocks for the preparation of conjugated oligomers and polymers, potential candidates for ONL applications. By the combination of these aromatic amines showing hole transporting properties with vinyl segments with strong emissive properties, a new class of electroactive conjugated materials can be generated. The tertiary amine units are not interrupting the conjugation of the principal chain in these compounds, the pair of electrons of the nitrogen atom contributing to the increase in effective conjugation and the double vinyl bonds creating 'conjugated bridges' between the aromatic units [31,32].

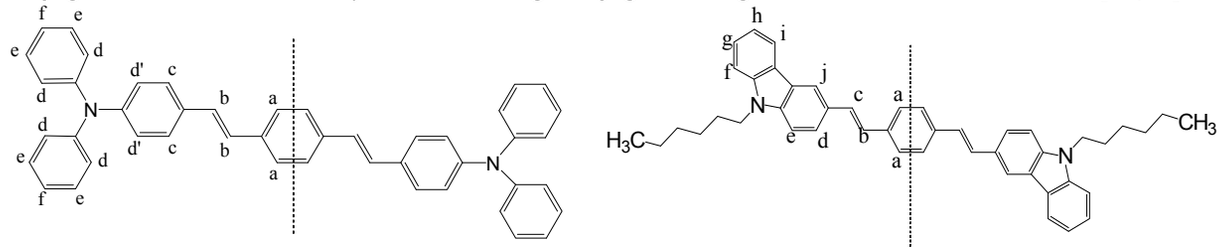

a) b)

Figure 7: Chemical structures of the oligomers L78:1, 4-bis [4-(N,N′-diphenylamino)phenylvinyl] benzene (a); L13: 3, 3′-bis (N-hexylcarbazole)vinylbenzene (b) [31].

Figure 7. Chemical structures of the oligomers L78: 1, 4-bis [4-(N, N′-diphenylamino)phenylvinyl] benzene (a); L13: 3, 3′-bis (N-hexylcarbazole)vinylbenzene (b) [31].

Some recent works have emphasised that symmetrically substituted organics D-π-D with donating groups situated at the ends linked by conjugated bridges, similar to those mentioned above, show important advantages, among which the large TPA cross-section [33, 34] and high transmission in visible range sustaining the generation of significant ONL phenomena.

Two arylenevinylene oligomers, L78 and L13, have been synthesised by Witting condensation using the following starting reagents: 4-formyltriphenylamine and N-hexyl-3-formylcarbazole and phosphonium salt of 1,4-bis(chloromethyl)benzene [31,35].

The chemical structure of the synthesised trans-arylenevinylene oligomers L78 and L13 has been evidenced correlating the FTIR measurements data presented in Figure 8 and Raman measurements data presented in Figure 9. The FTIR spectra shown in Figure 8 evidence the characteristic bands for the chromophoric groups in oligomers powder: ring in-plane bending vibration of the mono-substituted phenyl ring (ν_C-ν_C) situated at 1590–1598 cm^{-1}; phenyl rings (C=C) situated at 1505–1586 cm^{-1}; normal vibration with important contribution from C–N stretching coordinates situated at 1316–1332 cm^{-1} and 1030–1190 cm^{-1}; out-of-plane (wagging) vibration of the hydrogen atoms linked

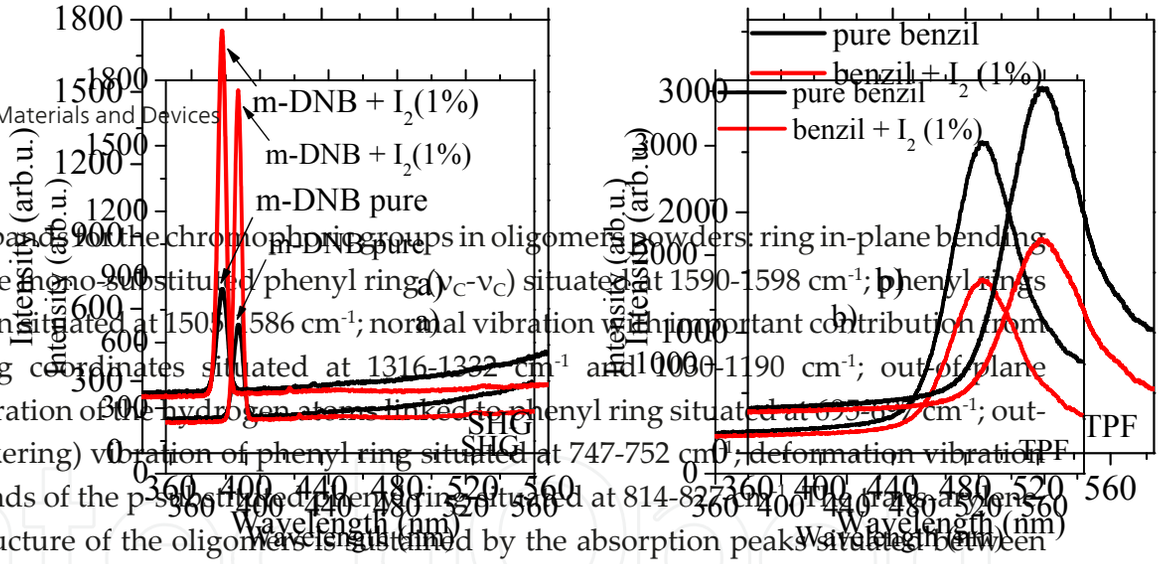

characteristic bands of the chromophoric groups in oligomers powders: ring in-plane bending vibration of the mono-substituted phenyl ring (ν_C-ν_C) situated at 1590-1598 cm^{-1}; phenyl rings (C=C) vibration situated at 1505-1586 cm^{-1}; normal vibration with important contribution from C-N stretching coordinates situated at 1316-1332 cm^{-1} and 1090-1190 cm^{-1}; out-of-plane (wagging) vibration of the hydrogen atoms linked to phenyl ring situated at 695-699 cm^{-1}; out-of-plane (puckering) vibration of phenyl ring situated at 747-752 cm^{-1}; deformation vibration of the C-H bonds of the p-substituted phenyl ring situated at 814-827 cm^{-1}. The polyparaphenylene levinylene structure of the oligomers is sustained by the absorption peaks situated between 960 and 962 cm^{-1} corresponding to the out-of-plane bending vibration of HC=CH [35].

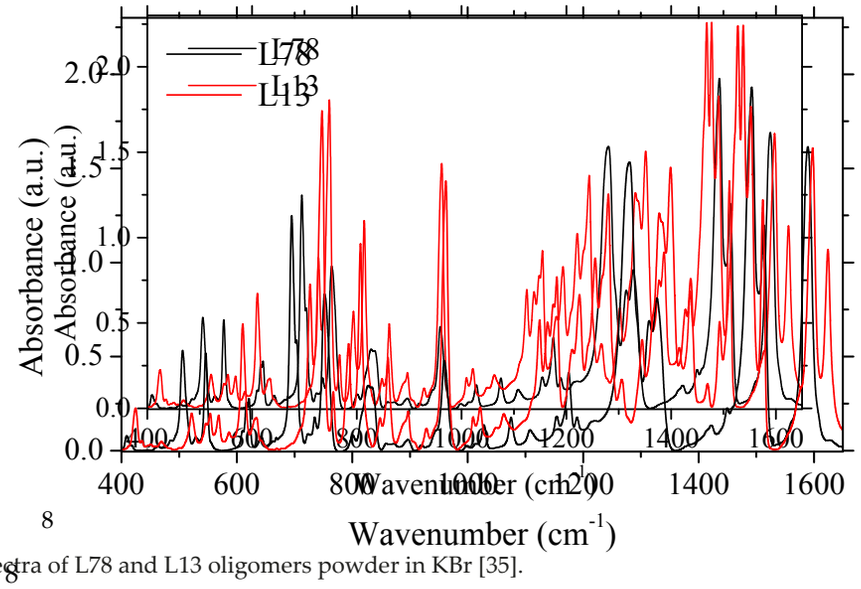

Figure 8. FTIR spectra of L78 and L13 oligomers powder in KBr [35].

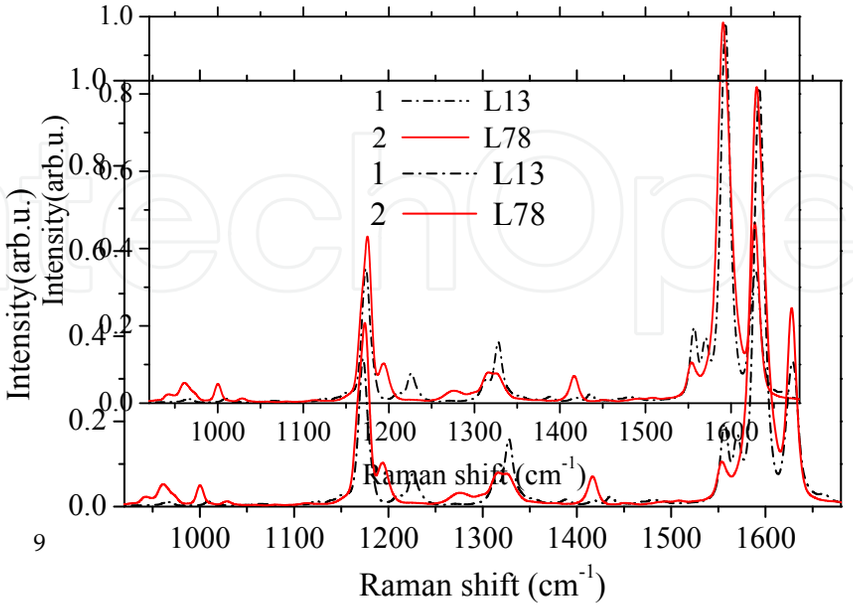

Figure 9. Raman spectra of L78 and L13 oligomers powder [31].

http://dx.doi.org/10.5772/60926

In Figure 9 are presented the Raman spectra which have offered complementary details about the characteristic bands for the chromophoric groups in oligomers powders: C-N stretches with associated C-C stretches in both L78 and L13 attributed to 970 cm^{-1}; C-N stretches with associated large C-C stretches in both L78 and L13 attributed to 1174 cm^{-1}; large C-N stretches with associated C-C stretches in L78 attributed to 1280 cm^{-1}; quadrant stretch of phenyl rings with associated C-N stretches in both L78 and L13 attributed to 1590 cm^{-1}. In carbazole-based compounds like L13, supplementary peaks attributed to $C_{carbazole}$-N stretches appeared at: 1123 cm^{-1}, 1132 cm^{-1} and 1230 cm^{-1} [36]. The Raman spectra show most of the sharp narrow well-defined peaks in spectral range 900-1750 cm^{-1} and are determined by scattering on the internal vibration modes [31].

Thin films of the mentioned arylenevinylene oligomers have been prepared on different substrates (quartz, silicon/Si, titanium/Ti) using two methods: vacuum evaporation and MAPLE. The properties of the layers have been analysed considering both the particularities of the molecular structure and solid state packing.

The X-ray diffraction spectra drawn in Figure 10 show no diffraction peaks confirming that the film deposited by vacuum evaporation is mostly amorphous, the molecule being randomly oriented [31]. We can consider a very reduced degree of order (more significant in L13), associated with the presence of the small, broad peak situated at 2θ=20°. Because the peak is broad, a small grain structure is attributed to the film [31].

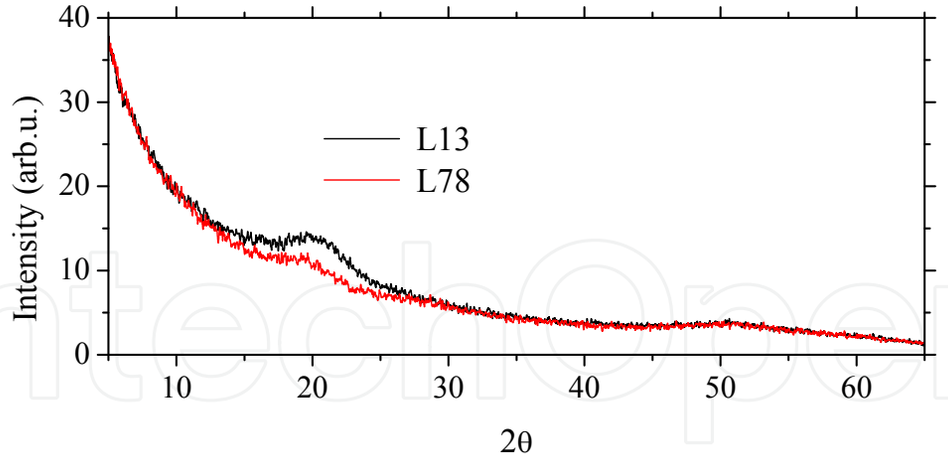

10

Figure 10. X-ray diffractograms for L78 and L13 oligomers thin films deposited by vacuum evaporation [31].

The SEM images of the oligomers films deposited by vacuum evaporation on Si presented in Figure 11 confirm the compact, small grain morphology evidenced by the broad XRD peak [31]. Some particular structures and aggregates, with acicular shape embedded in the L78 films and platelet shape in L13 films have also been evidenced [31]. This low density of randomly distributed structures has been developed during the deposition process.

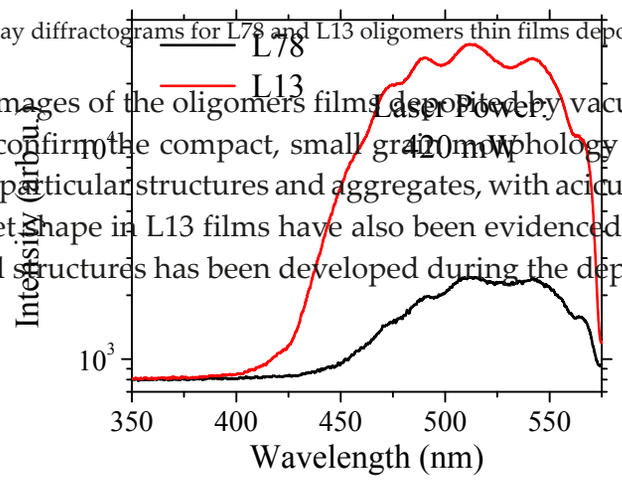

14

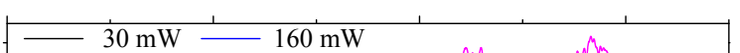

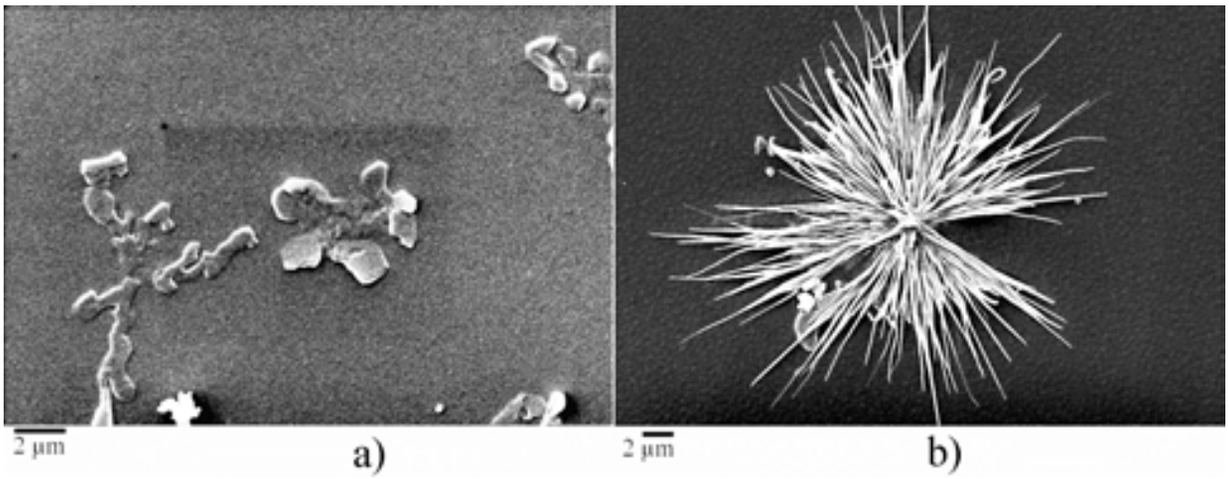

Figure 11. SEM images of L13 (a) and L78 (b) oligomer thin film deposited by vacuum evaporation [31].

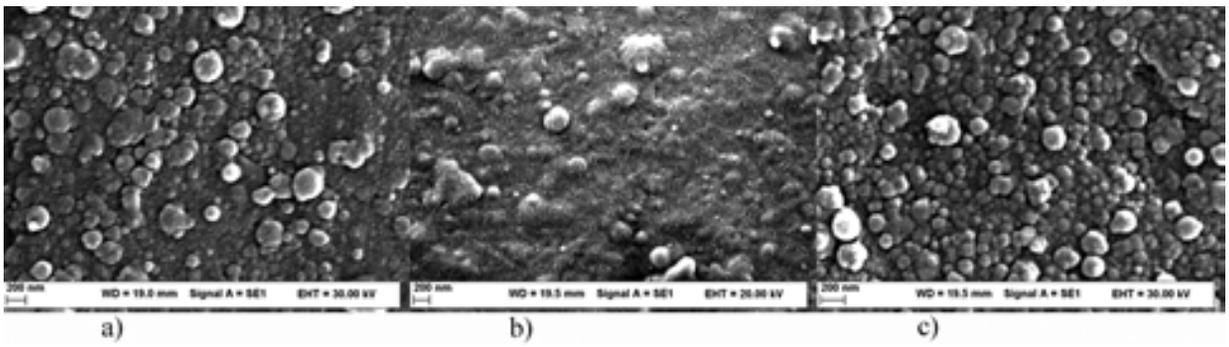

Figure 12. SEM images of L78 deposited by MAPLE from different solvents on different substrates: chloroform/quartz (a); dimethylsulphoxide (DMSO)/quartz (b); chloroform/Ti (c) [35].

The SEM images of the oligomers films deposited by MAPLE presented in Figures 12 and 13 have revealed different morphologies. The wrinkle morphologies of oligomers is generated by the inclusion of volatile solvent in the oligomer-rich surface favoured by the oligomer-solvent matrix droplets which appeared during the disintegration of the heated target [37].

In Figure 12 is evidenced the morphology of L78 thin films deposited by MAPLE both on quartz and on Ti using chloroform as solvent. L78 shows grains with a typical dimension up to 200 nm and larger-scale structures with different dimensions having spherical morphology randomly distributed in the layer [35]. When DMSO is used as solvent, the morphology of L78 on quartz is characterised by a lower density of spherical structures [35].

On the contrary, the films of L13 deposited on quartz have shown a morphology characterised by grains randomly distributed, as it is presented in Figure 13. The density of these grains has increased when the solvent was DMSO. A lower density of large spheres has been evidenced in the films of L13 deposited on Ti substrate using chloroform [35]. We can conclude that the morphology of the oligomers thin films depends on the deposition method, solvent and substrate.

http://dx.doi.org/10.5772/60926

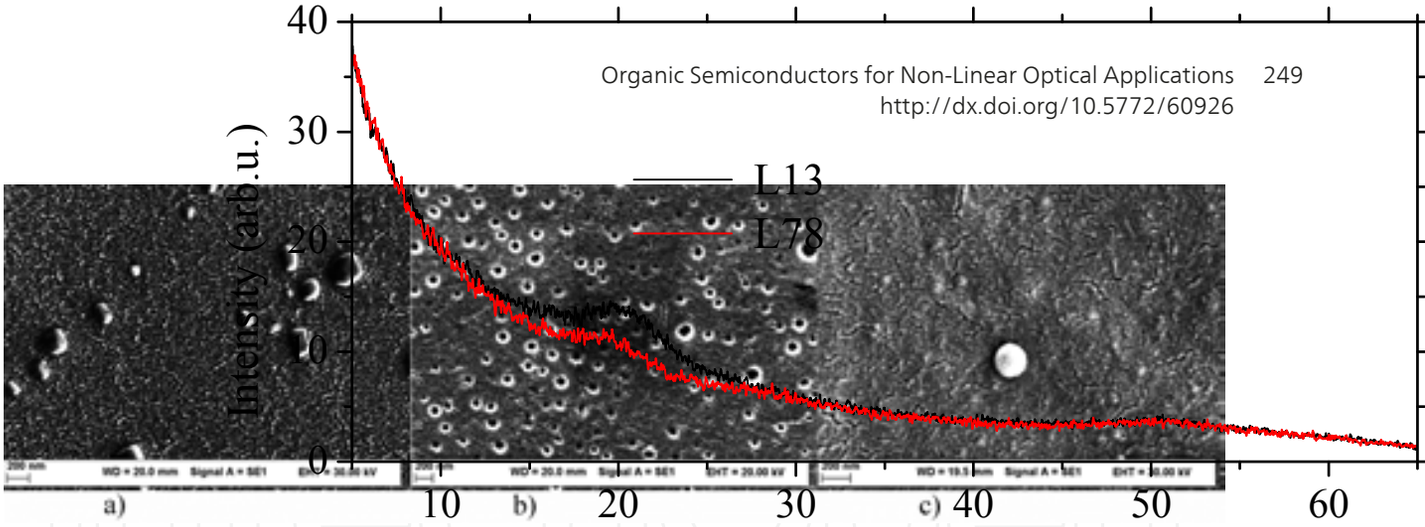

Figure 13. SEM images of L13 deposited by MAPLE from different solvents on different substrates: chloroform/quartz (a); DMSO/quartz (b); chloroform/Ti (c) [35].

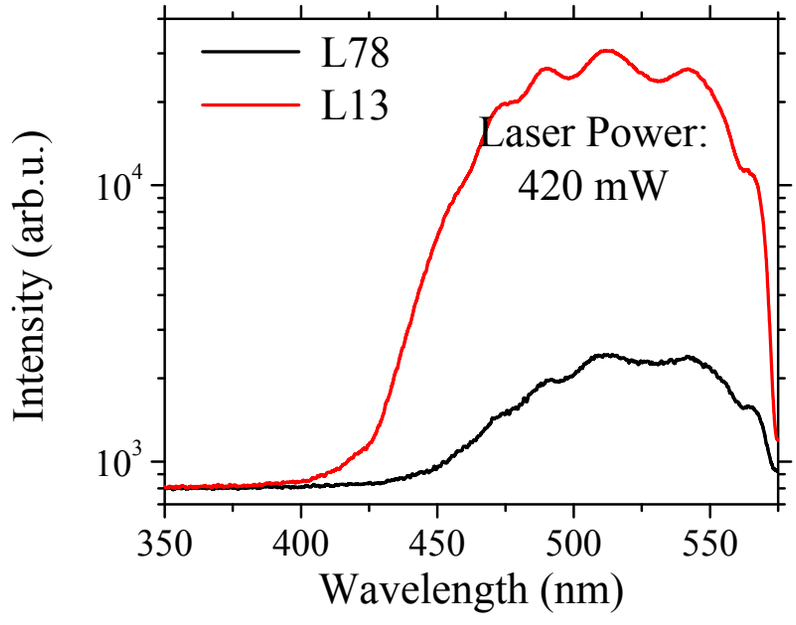

Figure 14. Fluorescence emission induced by two-photon absorption in oligomers L78 and L13 thin films deposited by vacuum evaporation on Si [31].

The shape of the TPF spectra and the position of the emission peaks correspond to those associated with the usual linear fluorescence spectra. This behaviour confirms that linear fluorescence and the TPF are generated by the relaxation of the system from the same excited state [31].

The optical properties of the MAPLE layers have been analysed in correlation with the molecular structure of the compounds, and the effects of the layer morphology determined by the solvent on the deposition process and on the resultant CNL processes have been emphasised.

Figure 14 revealed a strong TPF band centred on 525 nm in both oligomers, L78 and L13, thin films deposited by vacuum evaporation on Si. For high-intensity laser beam, the absorption of two photons with λ = 800 nm corresponding to the excitation wavelength of the laser, λ =

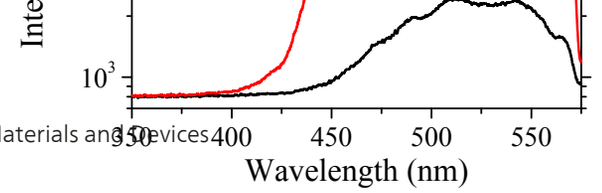

14

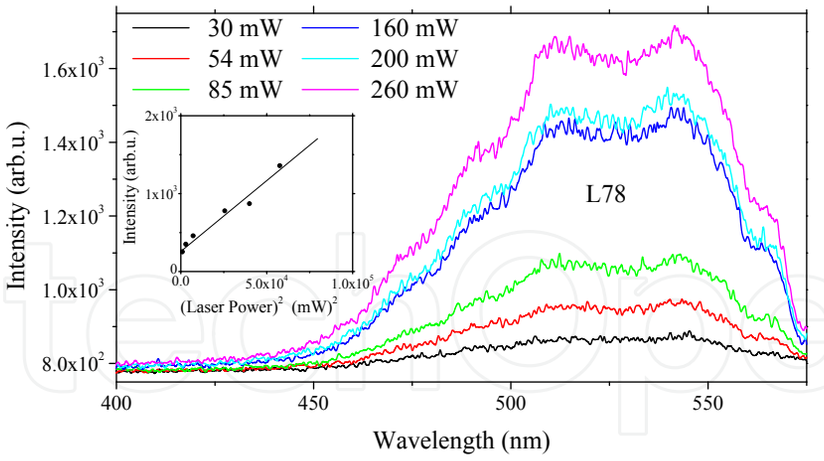

15

Figure 15. Dependence of TPF on laser power for L78 films deposited by vacuum evaporation on Si [31].

800 nm, could be replaced by the absorption of one photon with $\lambda = 400$ nm. After the absorption of one photon of 800 nm, the molecules of L78 and L13 do not have the time to relax because the duration of the laser pulse is very short, in the fs domain. Meanwhile, it absorbed the second photon of 800 nm and the molecular system was excited in a state from which it relaxed radiatively by TPF. For L78 and L13 using the same power of the excitation laser, 420 mW, we have obtained different intensity of TPF band, as a consequence of different focalisation regime of the laser beam [31].

The relation $I(2\omega) \propto (\chi^{(2)})^2 P_{(\omega)}^2$ [39] where P is the average power of the pulsed laser gives a simplified expression of the SH intensity. Therefore, a measure of the ONL behavior of the material can be given by the slope of the plot $I(2\omega)$ versus P_ω^2 presented in Figure 15 and 16.

The quadratic dependence between the fluorescence signal of the L78 thin films and the laser excitation power, as emphasised in Figure 15, with the slope ~2 at laser power <260 mW, confirms the presence of the ONL phenomenon and the two-photon nature of the excitation [31, 38].

The SHG, presented in Figure 16, induced by the ultra-intense focused beam of a femtosecond laser in a reflection configuration, has been used to compare the second-order ONL coefficients of the oligomer L78 and L13 thin films deposited on optically inactive Ti substrates by MAPLE [35].

Both oligomers thin films deposited on an optically inactive substrate have shown nearly equal values of the second-order ONL coefficients and these oligomers are similar from this point of view, when are irradiated with a low-power laser beam <100 mW. At laser powers higher than 100 mW was emphasised a deviation from the linear behaviour and the saturation of the SH attributed to significant changes in polarisability determined by thermally induced conformational changes of the side chain in oligomer molecules. These changes induced under the effect of absorbed laser radiation determine the reorientation of the dipoles and changes in polarisability of the material.

http://dx.doi.org/10.5772/60926

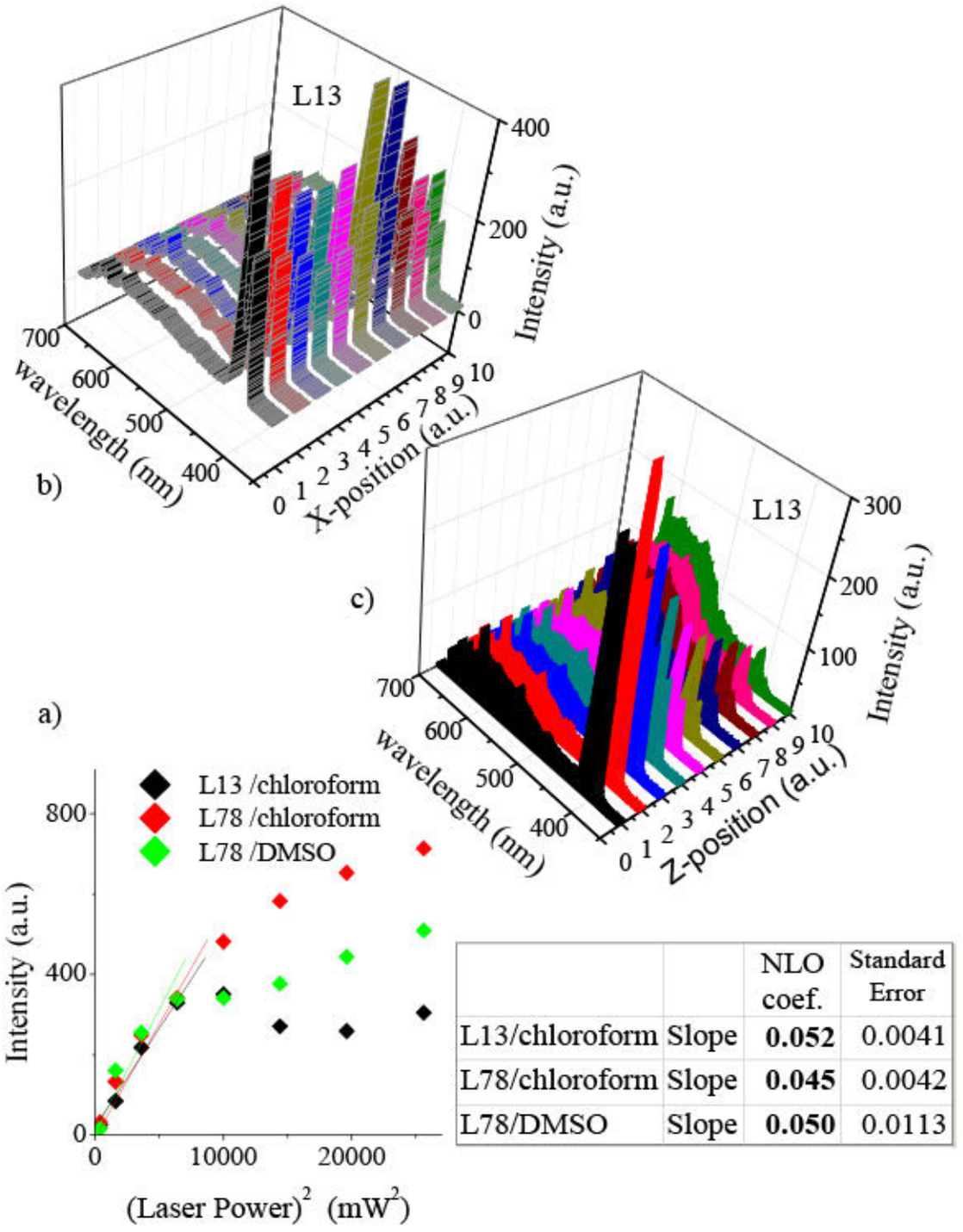

		NLO coef.	Standard Error
L13/chloroform	Slope	**0.052**	0.0041
L78/chloroform	Slope	**0.045**	0.0042
L78/DMSO	Slope	**0.050**	0.0113

Figure 16. SH measurements in oligomers L78 and L13 thin films deposited by MAPLE on Ti substrate [35].

Using the scanning in z and x directions (z-scan and x-scan representation) for oligomer L13 thin films, a broad TPF band with a peak at 650 nm which became more intense when the laser spot is focused inside the sample has been revealed. This confirms that TPF is a process taking place in the volume of the sample. The SH signal is stronger at the surface of the sample and

therefore could be altered by the surface morphology determined by the deposition experimental conditions including the solvent selected for the preparation of the MAPLE target [35].

Using the scanning in z and x directions (z-scan and x-scan representation) for oligomer L13 films, a broad TPF band with a peak at 650 nm which became more intense when the laser spot focused inside the sample has been revealed. This confirms that TPF is a process taking place in volume of the sample. The SH signal is stronger at the surface of the sample and therefore could altered by the surface morphology determined by the deposition experimental conditions including the solvent selected for the preparation of the MAPLE target [35].

3.2. Thin films based on maleimidic derivatives

Theoretical studies of the molecular structures with π-conjugation, containing functional groups having donor and acceptor properties, have revealed high first-order molecular hyperpolarisabilities and therefore these compounds seem adequate for the generation of ONL phenomena and manufacturing of thin-films-based optical devices for low-cost technology related to emerging photonic data processing, such as tunable wavelength systems filters, remote sensing, small-angle beam steering, high-bandwidth optical switches and modulators [40]. There are different ways to improve the generation of ONL phenomena from the increase in the strength of the electron donor and acceptor groups to increase in the length of the conjugated core and decrease of the ground state aromatic character [41]. The polarity of the monomers depends on the groups that substitute hydrogen in the benzenic nucleus and on the difference in electronegativities between these groups [42]. The selected maleimidic monomers contain dipolar segments determined by intramolecular electron withdrawing (donor) group and electron acceptor group and are characterised by the lack of balance between the effects of the substituent groups which determines the asymmetry in the distribution of electronic charges [42].

Theoretical studies of the molecular structures with π-conjugation, containing functional groups having donor and acceptor properties, have revealed high first-order molecular hyperpolarisabilities and therefore these compounds seem adequate for the generation of ONL phenomena and manufacturing of thin-films-based optical devices for low-cost technology related to emerging photonic data processing, such as tunable wavelength systems filters, remote sensing, small-angle beam steering, high-bandwidth optical switches and modulators [40]. There are different ways to improve the generation of ONL phenomena from the increase in the strength of the electron donor and acceptor groups to increase in the length of the conjugated core and decrease of the ground state aromatic character [41]. The polarity of the monomers depends on the groups that substitute hydrogen in the benzenic nucleus and on the difference in electronegativities between these groups [42]. The selected maleimidic monomers contain dipolar segments determined by intramolecular electron withdrawing (donor) group and electron acceptor group and are characterised by the lack of balance between the effects of the substituent groups which determines the asymmetry in the distribution of electronic charges [42].

The amidic derivatives monomers with the chemical structure presented in Figure 17 have been synthesised from maleic anhydride and a nitro aniline derivative with substituent groups showing different electronegativities, R [-NH-; -NH-NH-]; R1 [-COOH; -NO_2; -CN]; R2 [-NO_2]. The synthesis has implied the opening of the anhydridic cycle in dimethylformamide (DMF) at room temperature (A1, A2, A3, A5 and A6) and at higher temperature, 50°C, (A7) under weak stirring for 2 hours. The monomers have precipitated in ice and have been separated by filtration and recrystallisation from methanol [29].

The amidic derivatives monomers with the chemical structure presented in Figure 17 have been synthesised from maleic anhydride and a nitro aniline derivative with substituent groups showing different electronegativities, R [-NH-; -NH-NH-]; R1 [-COOH; -NO_2; -CN]; R2 [-NO_2]. The synthesis has implied the opening of the anhydridic cycle in dimethylformamide (DMF) at room temperature (A1, A2, A3, A5 and A6) and at higher temperature, 50°C, (A7) under weak stirring for 2 hours. The monomers have precipitated in ice and have been separated by filtration and recrystallisation from methanol [29].

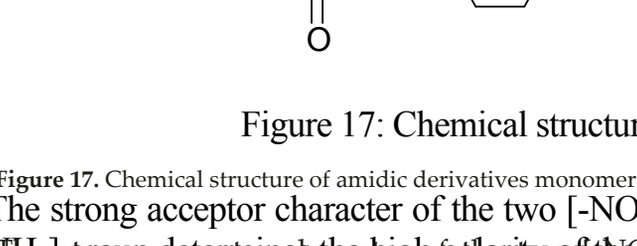

(A1) R: -NH-; R_1=-COOH; R_2:-H;
(A2) R: -NH-; R_1=-NO_2; R_2:-H;
(A3) R: -NH-; R_1=-CN; R_2:-H;
(A5) R: [-NH-]; R_1 and R_2: [-NO_2];
(A6) R: [-NH-NH-]; R_1 and R_2: [-NO_2];
(A7) R: [-NH-NH-]; R_1 and R_2: [-NO_2].

Figure 17: Chemical structure of amidic derivatives monomers [29,40].

Figure 17. Chemical structure of amidic derivatives monomers [29, 40].

The strong acceptor character of the two [-NO_2-] substituent groups compared to donor character of [-NH-] group determines the high polarity of the molecules in monomers (A6) and (A7) molecules.

The strong acceptor character of the two [-NO_2-] substituent groups compared to donor character of [-NH-] group determines the high polarity of the molecules in monomers (A6) and (A7) molecules.

3.2.1. Monomeric maleimidic derivatives thin films

Thin films of the selected monomers, presented in Figure 17, have been prepared by MAPLE, method assuring a better control of the film thickness by the number of pulses, surface morpholo by the fluence, amplified adhesion film/substrate and eliminating the possible source contamination because it is a non-contact procedure which can be integrated with other n contaminant processes [29]. For the preservation of molecular structure and deposition of clean f low fluences of 350–430 mJ cm^{-2} and a dimethylsulphoxide (DMSO) matrix have been used. thermalisation of the organic molecules was assured by a background gas, nitrogen at pres

http://dx.doi.org/10.5772/60926

3.2.1. Monomeric maleimidic derivatives thin films

Thin films of the selected monomers, presented in Figure 17, have been prepared by MAPLE, this method assuring a better control of the film thickness by the number of pulses, surface morphology by the fluence, amplified adhesion film/substrate and elimination of the possible source of contamination because it is a non-contact procedure which can be integrated with other non-contaminant processes [29]. For the preservation of molecular structure and deposition of clean films low fluences of 350-430 mJ cm^{-2} and a dimethylsulphoxide (DMSO) matrix have been used. The thermalisation of the organic molecules was assured by a background gas, nitrogen at pressure between 0.05 and 0.3 torr. The quality of the deposited layer was increased by heating the substrate at 150 °C or 250 °C during the deposition [29].

In the FTIR spectra of the powders of the above mentioned monomers have been evidenced strong and moderate characteristic bands as shown in Figure 18 attributed to the following sequences in aromatics, carboxyl acids and amides/imides: 1640 cm^{-1}, 1540 cm^{-1} to [-NH-] group; 1250 cm^{-1} to [-C=O] group; 1240 cm^{-1} to [-CN] group; ~840 cm^{-1} to [-CH=CH-] double bond; ~640 cm^{-1} to [-C-H-] single bond. The presence of the bands situated at 1390 cm^{-1} characteristic for amide and of the bands situated at 1100 cm^{-1} and 730 cm^{-1} corresponding to imides ring deformation confirm the simultaneous presence of amidic and imidic forms; bands situated in the range 650-800 cm^{-1} correspond to substituted benzene; bands situated in the range 1250-1300 cm^{-1} to symmetric stretching vibration of [-NO_2] group [40]. Most of the absorption peaks present in powder sample of a monomer have disapeared in thin-films sample of the same monomer because the films deposited by MAPLE are very thin (10-140 nm evaluated by spectroscopic ellipsometry [40]). As can be seen in Figure 18, most of the above mentioned absorption peaks have been evidenced in the thicker films of monomer A2 confirming the preservation during the MAPLE deposition of the monomer chemical structure [40].

The FTIR spectra of monomers A5 and A6 powder shown in Figure 19 have also revealed the presence of the characteristic bands situated at 3500-3200 cm^{-1} and 1620 cm^{-1} for [-COOH] group, 1580 cm^{-1} for [-NH-] group, 1250 cm^{-1} for [-C=O] group, ~840 cm^{-1} for [-CH=CH-] double bond and ~640 cm^{-1} for [-C-H-] single bond [29]. The disappearance, in the FTIR spectra of maleic anhydride, of the carbonylic band situated at 1860 cm^{-1} and the decrease, until disappearance, of the band situated at 1774 cm^{-1} sustain the formation of the maleamic acid and the presence of both amidic and imidic form of the monomer [29].

The well-defined peaks of Raman spectra in DMSO presented in Figure 20 situated between 800 cm^{-1} and 1750 cm^{-1} are atributted to scattering on internal vibrational modes and could be associated with the deformation of the molecules. The Raman shift peaks for different monomers corresponding to different substituent groups are: stretching vibration of [-NO_2] group in A2 and A7 situated at ~1340 cm^{-1}; stretching vibration of [-CN] group in A3 situated at 2220 cm^{-1}. The tri-substituted nucleus in A7 shows Raman shift peaks at 834 cm^{-1} and 1530 cm^{-1}. The peak situated at ~1600 cm^{-1} corresponds to stretching vibration of double bond -C=C-. Peaks situated at 75 cm^{-1} and 100 cm^{-1}, could be correlated with the external vibrations related to relative rotational or translational movement of molecules in solution [40]. The Raman spectra of A5 and A6 powders in DMSO drawn in Figure 21 show no significant differences,

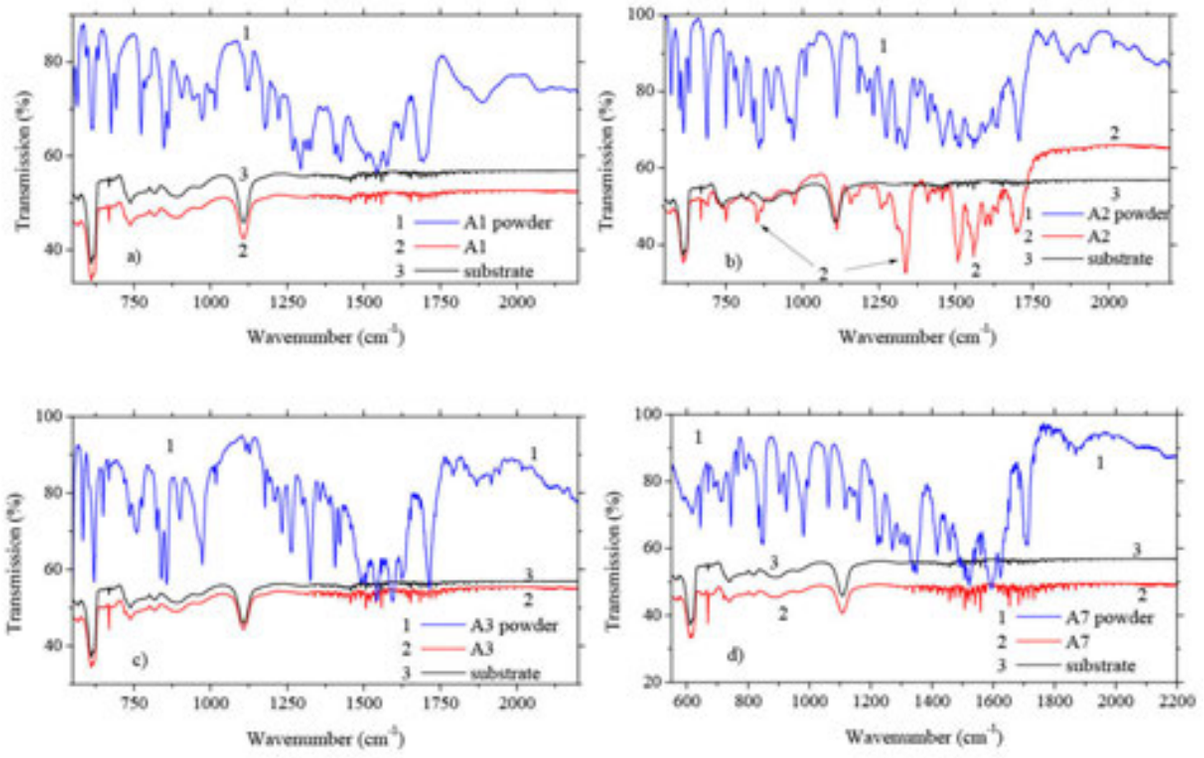

Figure 18. FTIR spectra of monomers powders and thin films deposited by MAPLE: monomer A1 (a); monomer A2 (b); monomer A3 (c); monomer A7 (d) [40].

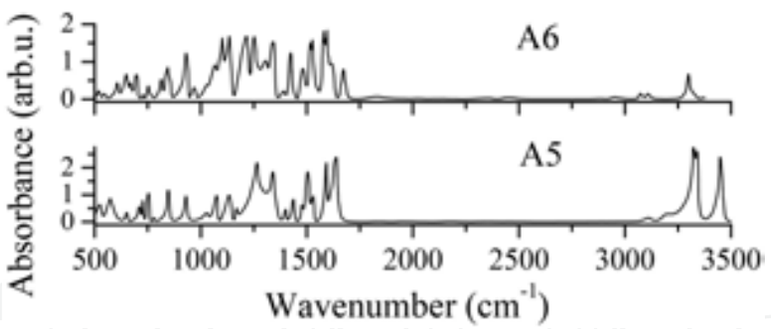

Figure 19. FTIR spectra of monomers A5 and A6 powder [29].

most of well-defined peaks being situated in the range 800-1700 cm^{-1} and being determined by the scattering on the internal vibration modes correlated with deformation of the molecules. The spectra are different in the range 1250-1350 cm^{-1} because of the stretching vibration of the C-C skeleton [29].

The peaks of 1, 2, 4-trisubstituted nucleus situated at 220 cm^{-1}, 375 cm^{-1}, 400 cm^{-1}, 480 cm^{-1} in Raman spectra of monomers are masked by the peaks corresponding to the solvent [29].

In the monomer thin films we have not evidenced Raman shift peaks because these films are very thin and can not generate a significant signal [40].

http://dx.doi.org/10.5772/60926

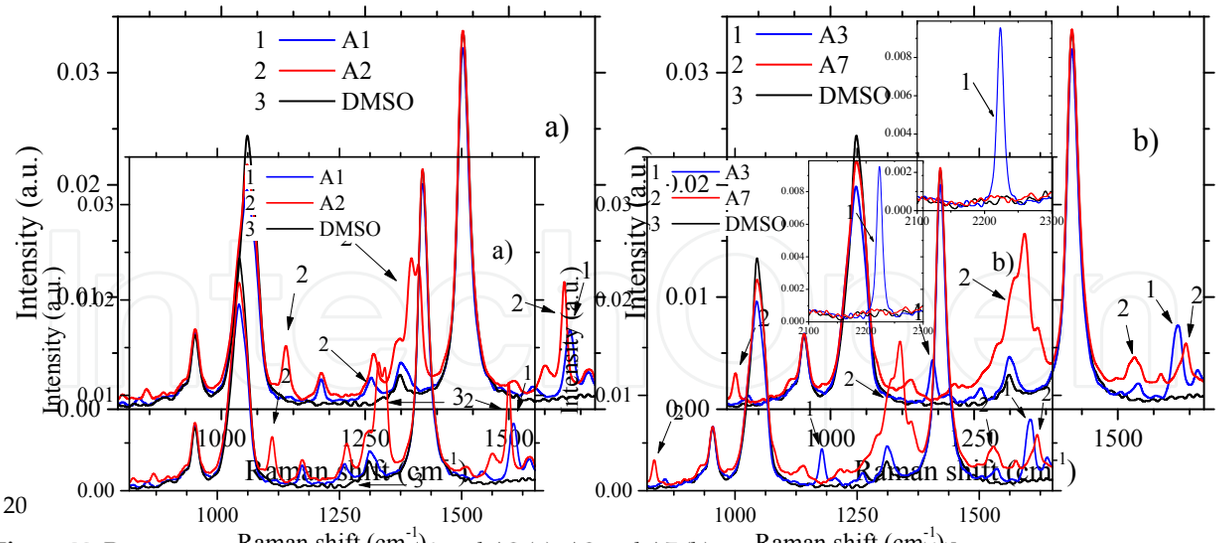

Figure 20. Raman spectra of monomers A1 and A2 (a), A3 and A7 (b) powders in DMSO [40].

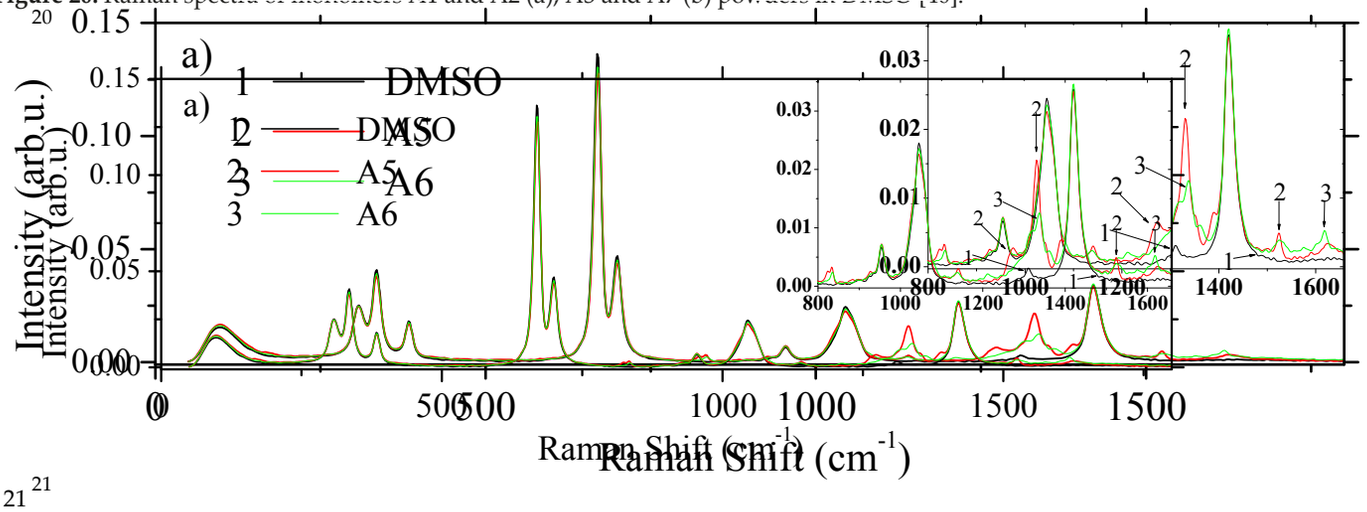

Figure 21. Raman spectra of monomers A5 and A6 powders in DMSO [29].

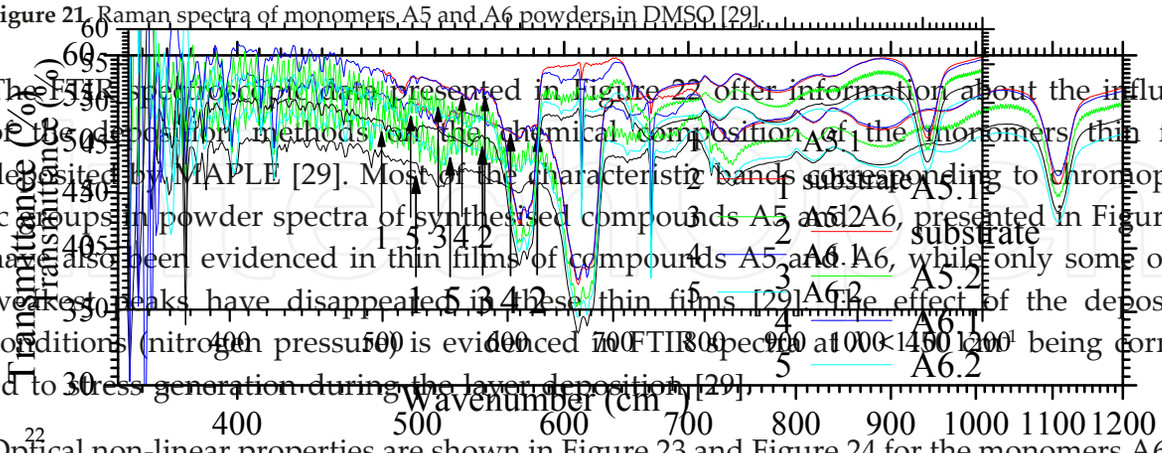

The FTIR spectroscopic data presented in Figure 22 offer information about the influence of the deposition methods on the chemical composition of the monomers thin films deposited by MAPLE [29]. Most of the characteristic bands corresponding to chromophoric groups in powder spectra of synthesised compounds A5 and A6, presented in Figure 19, had also been evidenced in thin films of compounds A5 and A6, while only some of the weakest peaks have disappeared in these thin films [29]. The effect of the deposition conditions (nitrogen pressure) is evidenced in FTIR spectra at 1000–1450 cm^{-1} being correlated to stress generation during the layer deposition [29].

Optical non-linear properties are shown in Figure 23 and Figure 24 for the monomers A6 and A7 thin films deposited by MAPLE. They are derived from a maleamic acid structure containing one [-NH-NH-] donor group and two [-NO_2] acceptor groups. These compounds combine the high polarisability and high dipolar momentum determined by the molecular structure with the good transparency and weak photoluminescence emission in the visible range preventing the re-absorption of the SH radiation and the decrease/screening of the SH signal [40]. In

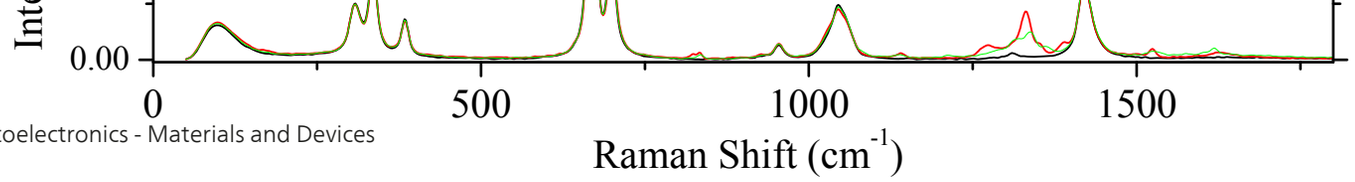

21

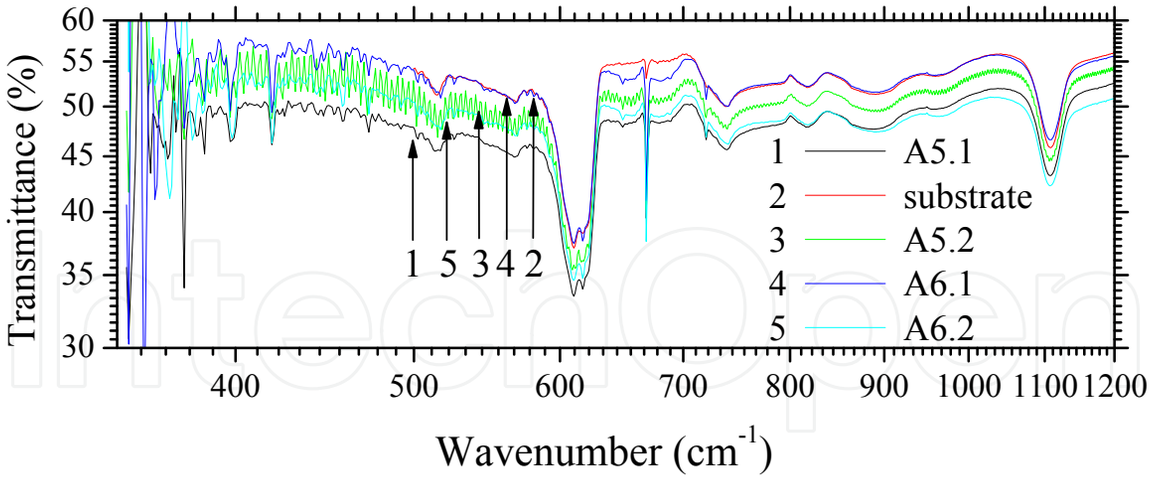

22

Figure 22. FTIR spectra of A5 and A6 thin films deposited at different nitrogen pressure: 0.05 torr A5.1 and A6.1; 0.2 torr A5.2 and A6.2 [29].

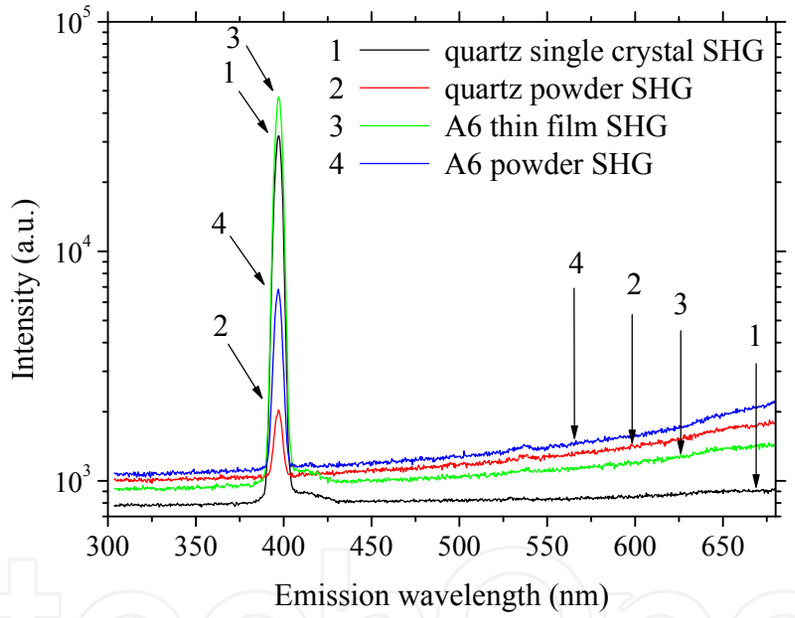

23

Figure 23. ONL effects in monomer A6 [29].

general, the para substitution in aromatic nucleus leads to highly polarisable charge transfer molecule with the tendency to crystallise in a centrosymmetric structure which do not favour the SH emission. In A6 and A7, the high [illegible] negativity of the substituent groups situated in position 1 [-NH-NH-] ar[illegible] the supplementary group situated in position 2 [-NO_2] acting on the[illegible]ke the centrosymmetry and favour the SH generation [29]. This combined effect of the asymmetry of the side groups and of delocalized, highly polarisable π electrons determines an acentric alignment of the aromatic nucleus in a special packing [43].

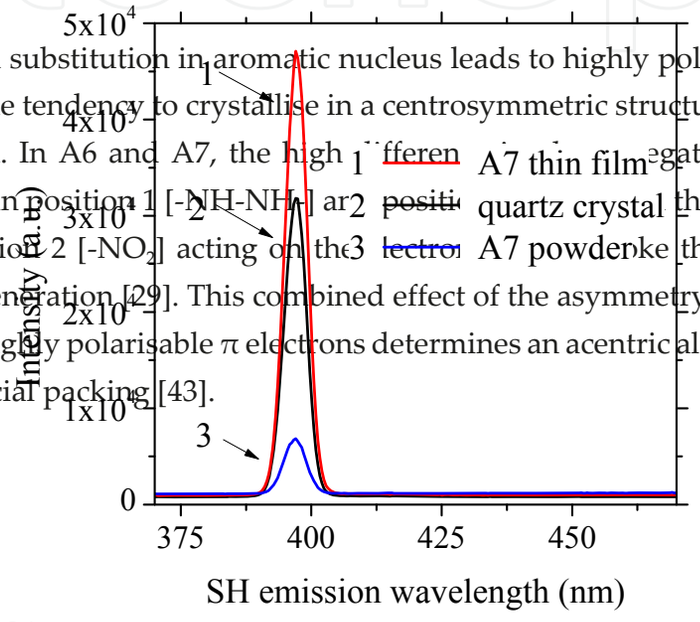

24

http://dx.doi.org/10.5772/60926

23

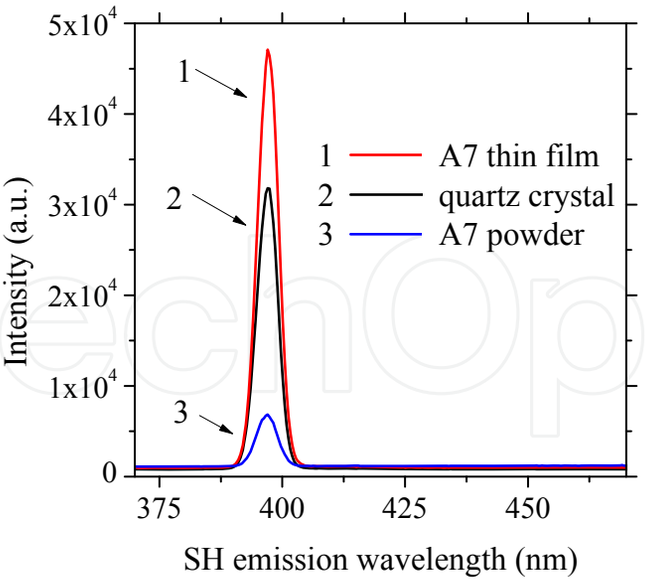

24

Figure 24. SH spectra of monomer A7 [40].

The SH signal of A6 and A7 thin films is compared with the signal given by A6 and A7 powders deposited on a substrate of aluminium which has no contribution to the SH emission. A quartz sample (crystal and powder) is used for comparison.

3.2.2. Maleimidic derivatives monomers in polycarbonate matrix as organic/organic composite thin films

The research in the field of composite materials based on rare earth (inorganic) and molecular/polymer (organic) matrix and organic/inorganic inclusions have received a special attention in the past years with the purpose to obtain a class of materials combining the advantageous properties of both components [44, 45]. Considering the advantage of organic compounds related to inexpensive thin-films preparation methods such as the deposition from solution by spin coating, the organic/organic composite materials offer an alternative for a large area of applications, including photonics.

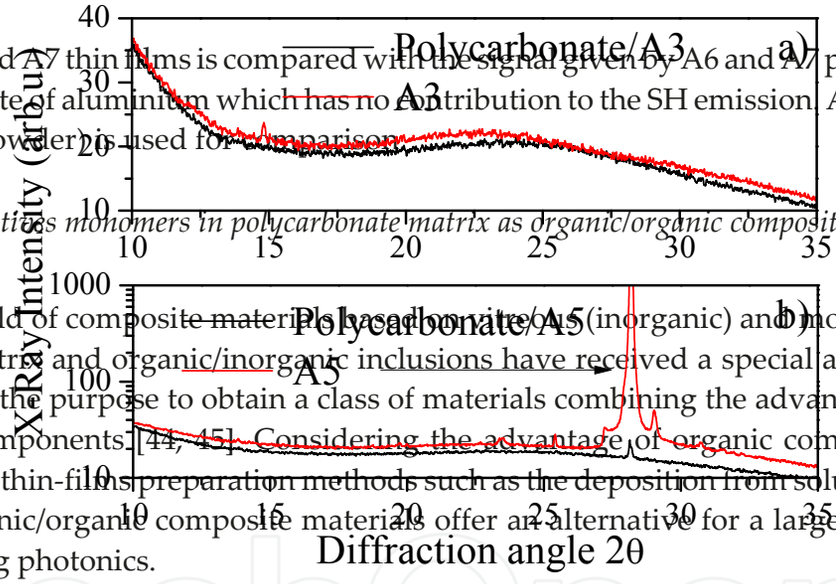

25

The polymeric matrices are easy to process because most of the polymers are soluble in ordinary solvents, show thermal and mechanical stability and are characterised by a large range of good transparency, homogeneous refraction index and efficient fluorescence mechanism. The interest is focused on the identification of π-conjugated systems with functional groups which improve the properties of the selected matrix considering the extension of the delocalised system of π-electrons, length of the conjugated chain and planarity of the molecule, factors involved in the generation of ONL phenomena [46]. The properties of the composite materials of the type 'host/guest' are determined by the solubility of the 'guest' molecule into the 'host' matrix.

We have selected a polymeric matrix of polycarbonate of bisphenol A showing a large transparency domain between 300 and 1100 nm and inclusions of monomers with maleamic acid structure such as A3 and A5, indicated in Figure 17. The composite films have been

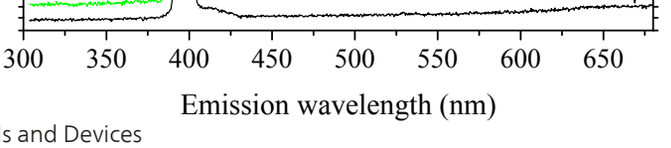

23

prepared from solution by spin coating on glass substrate successively cleaned with acetone and distillate water, using a solution containing both components: polymer in concentration of 0.09 g cm^{-3} or 0.250 g cm^{-3} and monomer in concentration varying from 0.01 g cm^{-3} to 0.25 g cm^{-3} in dimethylformamide (DMF) [47].

The solvent DMF has been selected considering the surface energy determined by contact angle measurements, the high solubility of both polycarbonate and mentioned monomers in DMF compared to DMSO and the volatility at room temperature. The experimental conditions for the preparation of films have been selected from macroscopic morphological consideration referring to the uniformity of the layer: t_1 = 6 s and v_1 = 1.13 krpm in the spreading step and t_2 = 10 s and v_2 = 2.7 krpm in the homogenisation step, for a weight ratio between monomer and polymer of 1/3 [47]. The effect of the matrix on the properties of monomer inclusions are evidenced comparing the properties of these films with those of the reference samples of monomers thin films prepared by vacuum evaporation.

24

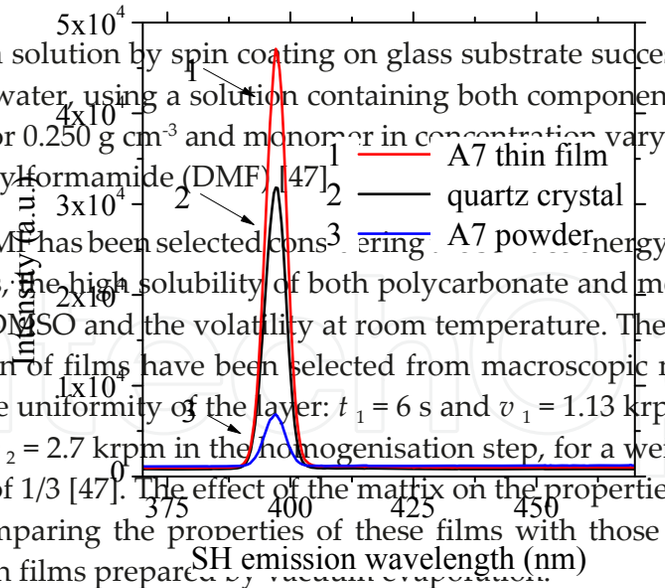

25

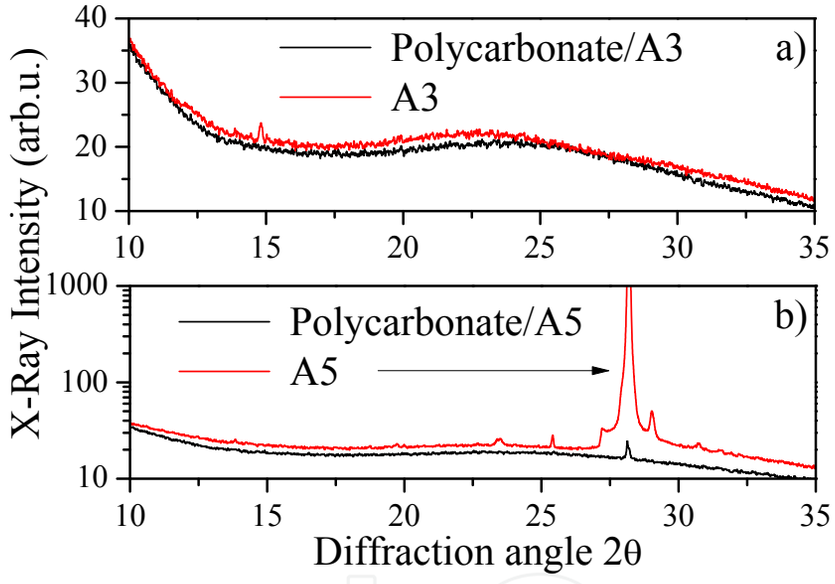

Figure 25. X-ray diffraction spectra of monomers A3 and A5 and polycarbonate/monomer (A3, A5) deposited on glass substrate [47].

An increased disorder in polycarbonate/monomer Ax with x = 3, 5 layer deposited by spin coating compared to monomer Ax with x = 3, 5 layer deposited by vacuum evaporation is confirmed by the X-ray diffractograms in Figure 25. The peak situated around 28° corresponding to dinitroaniline is present both in the spectrum of monomer A5 and in the composite based on the same monomer. The film of polycarbonate/A3 deposited on glass is mostly amorphous compared to the vacuum evaporated A3 film. The A3 film shows a small peak situated at 13° corresponding to cyano aniline and indicating a certain small degree of order (crystallisation) in the vacuum-evaporated film. The X-ray diffractograms have evidenced a preferential orientation of A5 monomer film which is partially preserved in composite polycarbonate/A5 film, compared to A3 and polycarbonate/A3 films showing a substantial disorder [47].

http://dx.doi.org/10.5772/60926

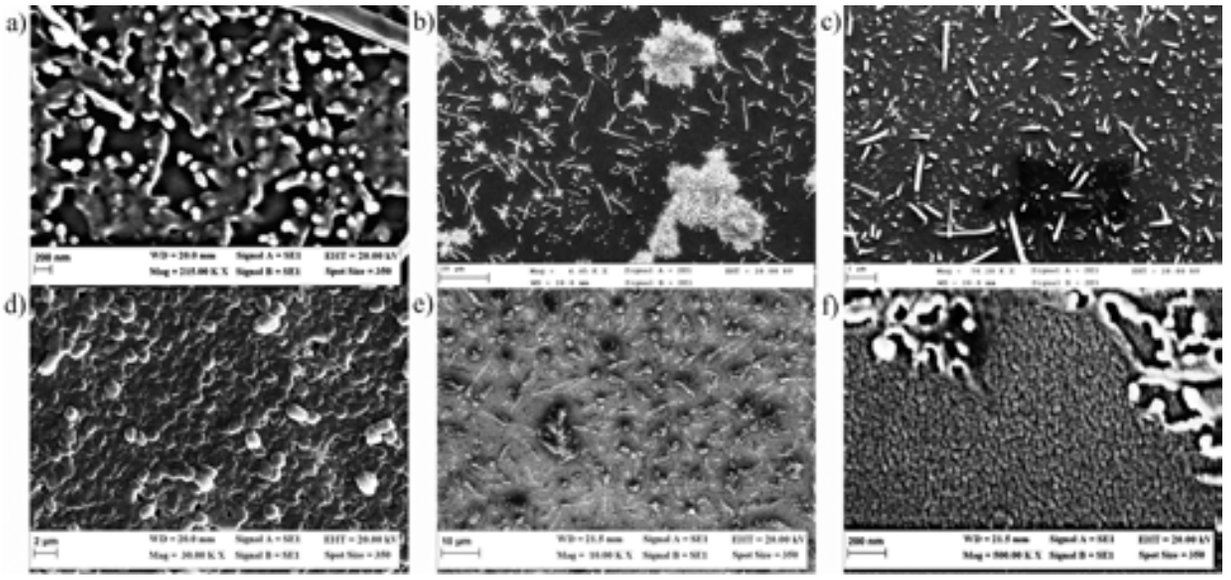

Figure 26. SEM images of monomers A3 (a) and A5 (d) films vacuum evaporated on glass and composite polycarbonate/A3 (b, c); A5 (e, f) layers deposited by spin coating on glass [47].

The SEM images presented in Figure 26 have evidence a continuous, compact organic layer deposited on glass, with large grain morphology for A5 and smaller grain morphology with lower packing density for A3 [47]. The composite layers have shown morphology characterised by 'grains' and 'grains clusters' which are homogeneously developed in the polymeric matrix that wets the glass substrate [47].

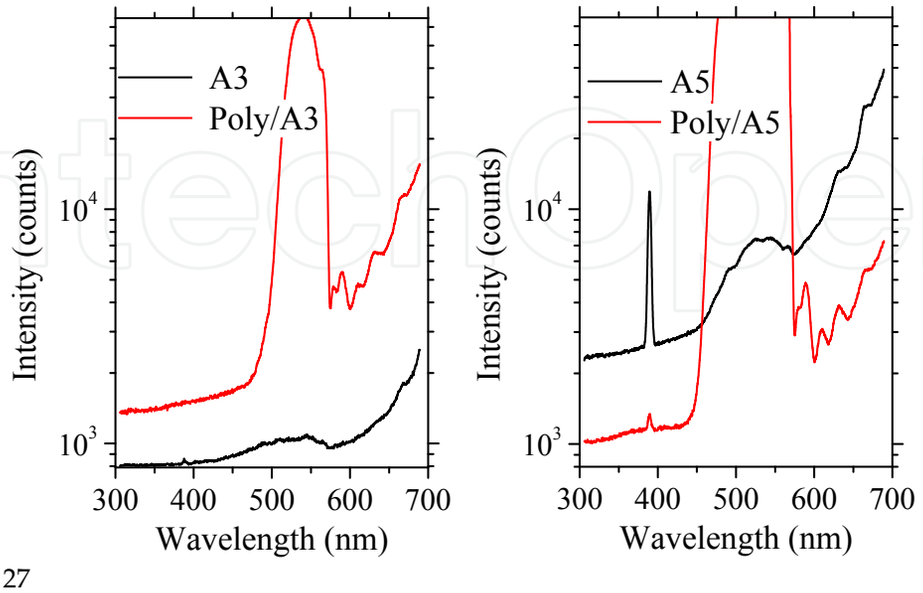

27

Figure 27. ONL effects in monomers (A3, A5) and polycarbonate/monomer (A3, A5) deposited on glass [47].

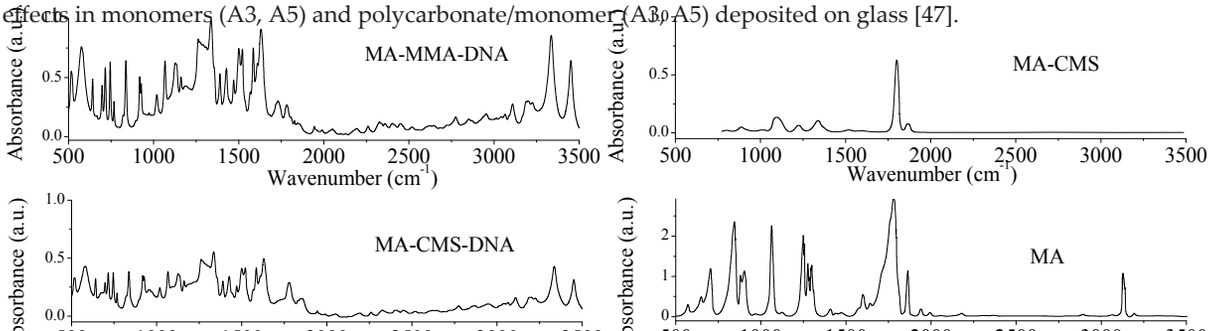

The emission spectra of the monomers thin films at illumination with a laser beam with λ = 800 nm presented in Figure 27 show an emission peak situated at 400 nm corresponding to SH. This signal is strongly affected by the surface properties like morphology. The larger grain morphology of A5, as shown in Figure 26, is associated with a stronger SH signal because of the lower loss by scattering compared to A3 showing smaller grain morphology. The SH emission is explained by an intense mezomeric effect determined by the difference in electronegativity of the substituent groups and a strong inductive effect between the strongly polarisable chromophoric groups -NO_2 and -CN coupled with the polarisable aromatic nucleus [47].

Polycarbonate/A3 and polycarbonate/A5 films show a strong signal situated between 475 and 600 nm attributed to TPF emission together with a decrease in SH signal which is affected by surface morphology of the layers deposited by spin coating. TPF is a volume process and it is not affected by the morphology of the surface [47].

3.3. Thin films based on functionalised copolymers

Another alternative to the inorganic compounds for ONL applications is represented by the polymers showing high non-resonant ONL properties. In polymeric materials containing dipolar chromophores, the macroscopic second-order optical non-linearity could be induced by intramolecular donors-acceptors groups. In these materials, either molecular fragments showing ONL properties are spread in a polymeric matrix or highly colored chromophores are attached covalently in two possible ways, as side chain or intercalated in the backbone of the polymer's chain [48]. High values of the non-linear coefficients can be obtained in a non-centrosymmetric packing by an acentric alignment of the molecules favoured by the structure of the side groups and/or polymer. This condition can be accomplished by an increased density of chromophores assured by the functionalisation of polymers (copolymers) with molecules containing highly polarisable conjugated electronic clouds [49, 41].

The structural and morphological particularities of the materials depend on the method selected for preparation (MAPLE and vacuum evaporation; solution deposition such as spin coating) and affect the properties of the materials.

We have studied two polymeric structures introduced in Figure 28, P1: MA-CMS-DNA synthesised by the copolymerisation of maleic anhydride (MA) with vinyl benzil chloride (MA-CMS) and subsequent functionalisation with 2, 4-dinitroaniline (DNA) and P2: MA-MMA-DNA synthesised by the copolymerisation of maleic anhydride and methylmethacrilate (MA-MMA) and subsequent functionalisation with 2, 4-dinitroaniline (DNA). Functionalised copolymers have been synthesised in a two-stages process: (1) polymerisation by precipitation initiated by azoizobutylnitrile in toluene at 80^{o}C for 2 h; (2) polymers grafting with ortho-, para-aniline derivatives in DMF by opening and closing of the anhydridic cycle at 120°C for 2 h [50-52, 29].

Thin films of grafted copolymers P1 and P2 have been prepared using different methods on different substrates like glass, cleaned in acetone, and etched/etched single silicon wafers, successively cleaned ultrasonically with acetone, hydrofluoric acid and distillate water [50].

(copolymers) with molecules containing highly polarisable conjugated electronic c
The structural and morphological particularities of the materials depend on the
preparation (MAPLE and vacuum evaporation; solution deposition such as spin
the properties of the materials.

http://dx.doi.org/10.5772/60926

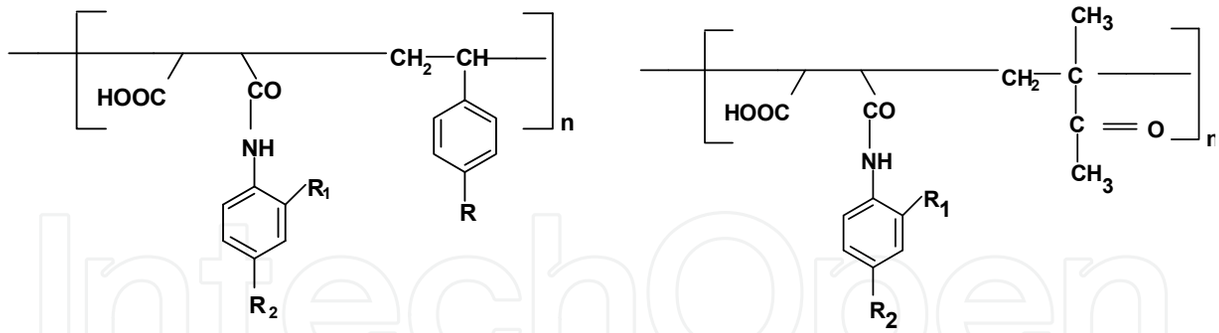

R: CH_2Cl
R1: NO_2
R2: NO_2

(a)

R1: NO_2
R2: NO_2

(b)

Figure 28: Selected copolymers: P1: MA-CMS-DNA (a); P2: MA-MMA-D

Figure 28. Selected copolymers: P1: MA-CMS-DNA (a); P2: MA-MMA-DNA (b) [50].

We have studied two polymeric structures introduced in Figure 28, P1: MA-CM
by the copolymerisation of maleic anhydride with vinyl benzil chloride (MA-CM
functionalisation with 2,4-dinitroaniline (DNA) and P2: MA-MMA-DNA s
copolymerisation of maleic anhydride and methylmethacrilate (MA-MMA
functionalisation with 2,4-dinitroaniline (DNA). Functionalised copolymers have
a two-stages process: (1) polymerisation by precipitation initiated by azoizobutyl
80°C for 2 h; (2) polymers grafting with ortho-, para-aniline derivatives in DM
closing of the anhydridic cycle at 120°C for 2 h [50–52, 29].
Thin films of grafted copolymers P1 and P2 have been prepared using different m
substrates like glass, cleaned in acetone, and etched/etched single silicon wafers, s
ultrasonically with acetone, hydrofluoric acid and distillate water [50].
Polymeric films have been deposited from solution by spin coating in a process i
(1) preparation of polymer solution in an adequate solvent; (2) deposition of th

Polymeric films have been deposited from solution by spin coating in a process involving two steps: (1) preparation of polymer solution in an adequate solvent; (2) deposition of the film by spin coating (spinning time 40 s for P1 and 30 s for P2; rotational speed 2.75 krpm for P1 and 0.65 krpm for P2 [50]) followed by homogenization (spinning time 20 s for P1 and 10 s for P2; rotational speed 2.75 krpm for P1 and 1.70 krpm [50]). We have selected DMF as solvent because it is characterised by a low evaporation rate and strong interactions with the native layer of SiO_2 covering the Si surface.

Polymeric thin films have also been prepared by vacuum evaporation at a temperature of 100-110°C for P1 and 80-90°C for P2 and a pressure between 1.2-1.9×10^{-5} mbar for P1 and 1.0-1.7×10^{-5} mbar for P2 [50]).

The characteristics of the films prepared by spin coating and vacuum evaporation have been compared with those of the films prepared by a laser-based technique, MAPLE [51, 29]. To avoid the deterioration in laser beam of the polymer characterised by weak chemical bonds, it is used a diluted frozen target with 1% polymer wt. in an adequate solvent, and a good absorption at the laser wavelength, in our experimental configuration λ=248 nm, namely DMSO [51]. The solution of polymer in DMSO is frozen in liquid nitrogen and this target is placed in the deposition chamber. The energy of the incident laser beam is absorbed mostly by the molecules of solvent, the target heats and the components of the target are simultaneously evaporated. The polymer deposits on a heated substrate while the volatile solvent is pumped away from the chamber. Low values of the fluencies (~0.4 J cm^{-2}) are necessary to avoid the fragmentation of the polymeric chain and decomposition of the photosensible organic compounds [53]. Beside fluence, other important experimental parameters are presented in Table 1 concentration of the target, nitrogen pressure, substrate temperature and number of pulses [51, 29].

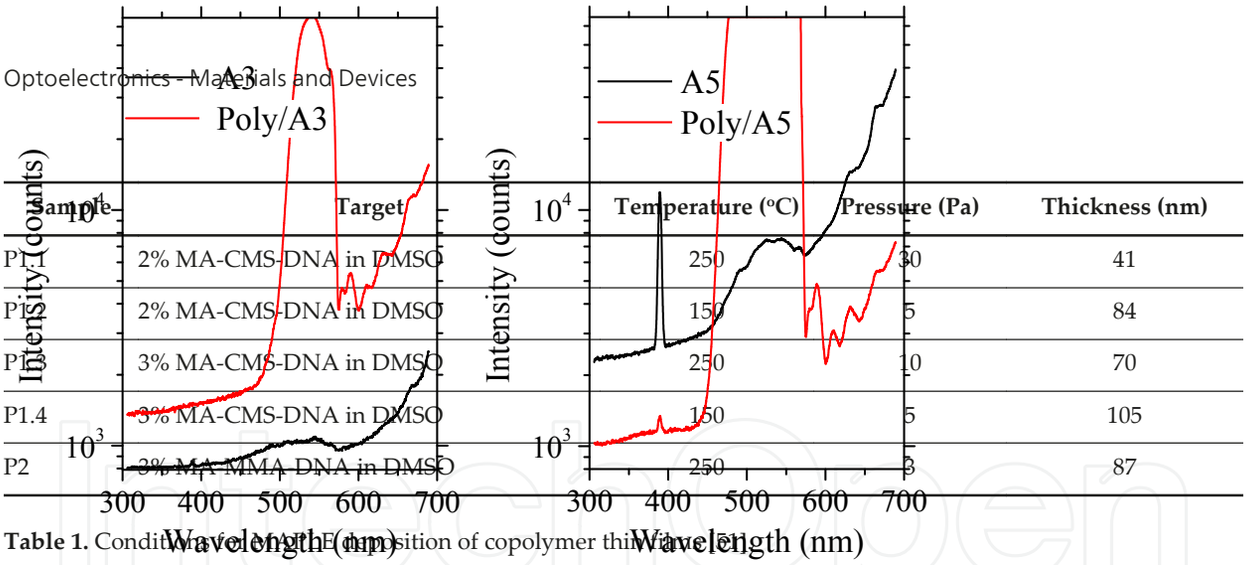

Sample	Target	Temperature (°C)	Pressure (Pa)	Thickness (nm)
P1.1	2% MA-CMS-DNA in DMSO	250	30	41
P1.2	2% MA-CMS-DNA in DMSO	150	5	84
P1.3	3% MA-CMS-DNA in DMSO	250	10	70
P1.4	3% MA-CMS-DNA in DMSO	150	5	105
P2	3% MA-MMA-DNA in DMSO	250	3	87

Table 1. Conditions for MAPE deposition of copolymer thin layers [29].

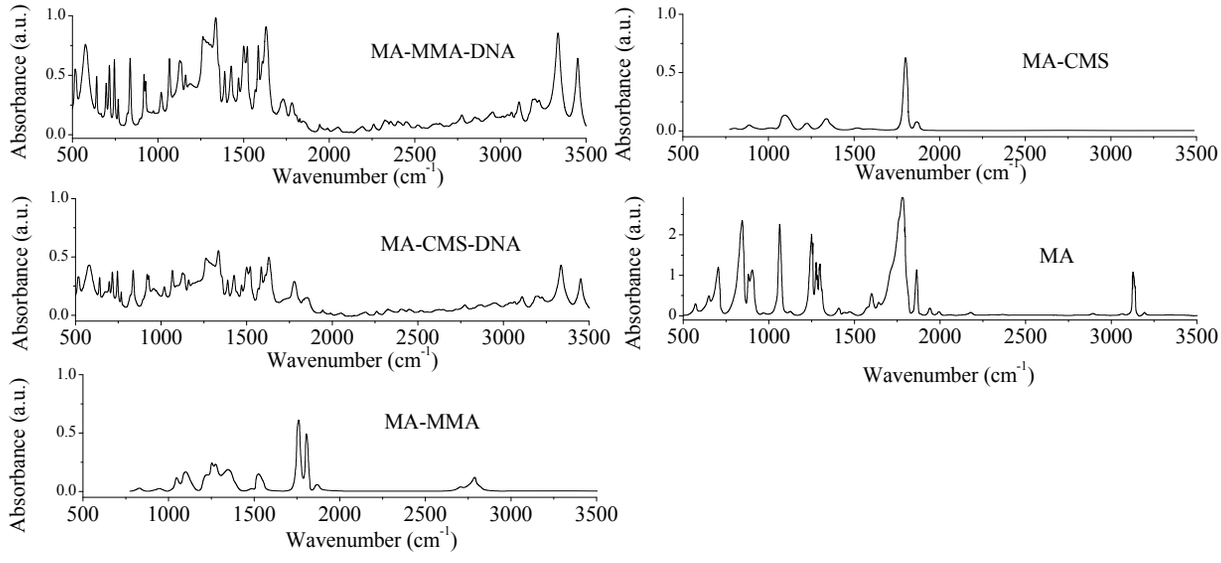

Figure 29. FTIR spectra of powder maleic anhydride (MA), copolymeric support (MA-CMS and MA-MMA) and dinitroaniline derivative functionalised copolymers (MA-CMS-DNA:P1 and MA-MMA-DNA:P2) [29].

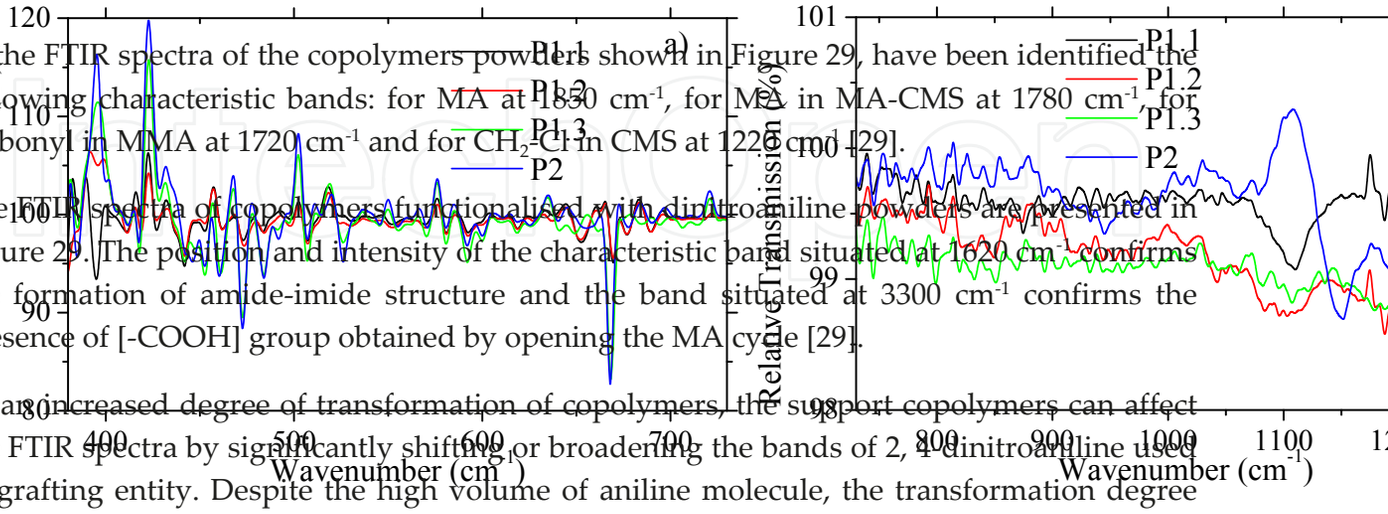

In the FTIR spectra of the copolymers powders shown in Figure 29, have been identified the following characteristic bands: for MA at 1830 cm^{-1}, for MA in MA-CMS at 1780 cm^{-1}, for carbonyl in MMA at 1720 cm^{-1} and for CH_2-Cl in CMS at 1220 cm^{-1} [29].

The FTIR spectra of copolymers functionalised with dinitroaniline powders are presented in Figure 29. The position and intensity of the characteristic band situated at 1620 cm^{-1} confirms the formation of amide-imide structure and the band situated at 3300 cm^{-1} confirms the presence of [-COOH] group obtained by opening the MA cycle [29].

At an increased degree of transformation of copolymers, the support copolymers can affect the FTIR spectra by significantly shifting or broadening the bands of 2, 4 dinitroaniline used as grafting entity. Despite the high volume of aniline molecule, the transformation degree of MA-MMA copolymer is higher ~16% compared to MA-CMS ~9% and can be explained by the higher accessibility of MA entities to the grafting units determined by the structure of the copolymer [29].

http://dx.doi.org/10.5772/60926

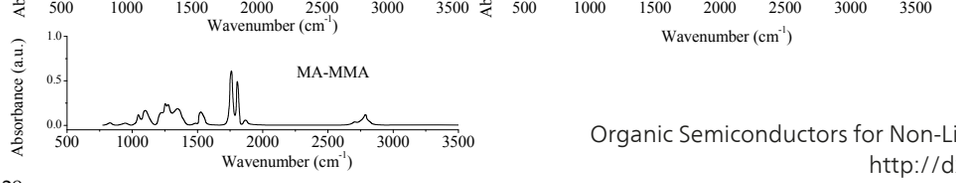

29

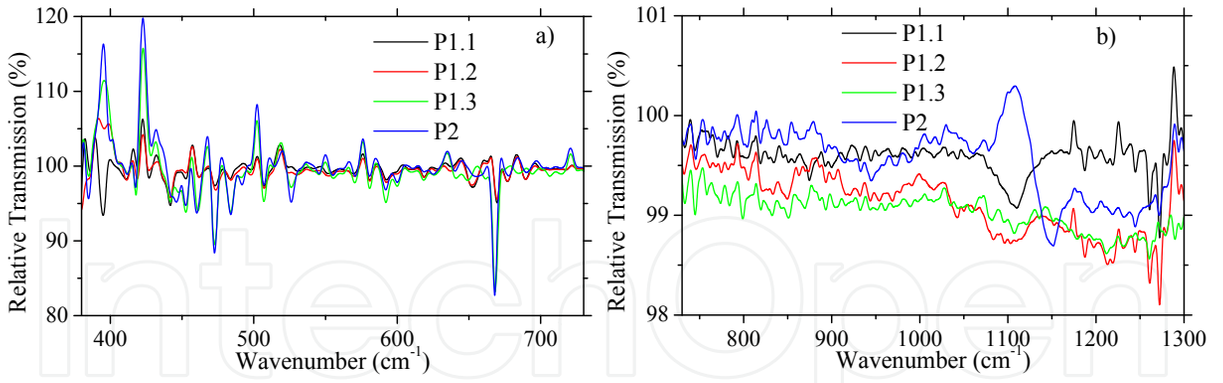

30

Figure 30. FTIR spectra of P1 and P2 films deposited on Si by MAPLE from DMSO in different spectral ranges: 380-730 nm (a); 730-1300 nm (b) [51].

The FTIR spectra presented in Figure 30 have evidenced the characteristic bands in P1 and P2 films deposited by MAPLE, attributed to 2, 4-dinitroaniline which has been used for the functionalisation of copolymers: 1270 cm^{-1} carbonyl (C=O); 900 cm^{-1} double bond (CH=CH); 675 cm^{-1} single bond (C-H); 1390 cm^{-1} amide group; 1100 cm^{-1} imide group (ring deformation). The last two bands confirm the presence of amidic and imidic forms. The strong or moderate absorption band situated between 900 and 600 cm^{-1} is attributed to bending vibration in aromatics, carbonyl acids and amides. The absorption band situated between 600 and 400 cm^{-1} can be attributed to meta-substituted aromatics. Other absorption bands are: 1250-1300 cm^{-1} the symmetric stretching vibration of NO_2; ~1240 cm^{-1} aromatic CN bonding; 1175 cm^{-1} CH in plane deformation. The formation of copolymer MA-CMS is confirmed by the presence of the absorption band situated at ~1210 cm^{-1} corresponding to CH_2-Cl bond in CMS. The bands situated at ~1150 cm^{-1} and ~1260 cm^{-1} corresponds to maleic anhydride in methyl methacrylate. The band characteristic for 2, 4-dinitroaniline could be broadened or shifted under the effect of the support copolymers depending on the degree of transformation [50, 51]. The support copolymers can affect as well the FTIR spectra of MAPLE deposited films by significantly shifting or broadening the bands of the 2, 4-dinitroaniline at high degree of transformation of copolymers.

There are no significant differences between the functionalised copolimers films deposited by vacuum evaporation and spin coating, excluding the possibility of polymer decomposition during the evaporation process, a high-temperature process compared to spin coationg, a room temperature process. New absorption peaks corresponding to new bonds have not been evidenced in the polymeric films deposited by vacuum evaporation. Even no chemical reaction took place during the evaporation, it could be possible a fragmentation of the copolymeric support, maintaining intact the chromophoric groups. This is sustained by the similarity between the shape of the FTIR spectra of the evaporated polymeric films and of the MA-DNA monomer fragment [29, 50].

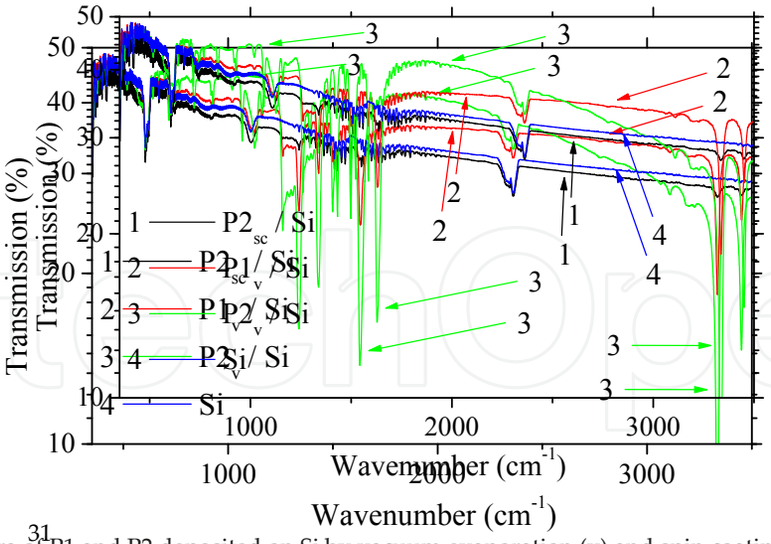

Figure 31. FTIR spectra of P1 and P2 deposited on Si by vacuum evaporation (v) and spin coating (sc) [50].

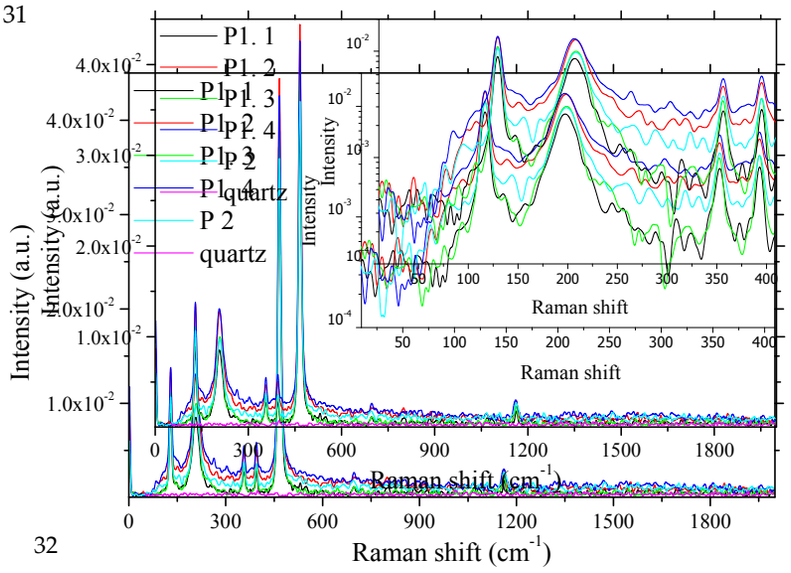

Figure 32. Raman spectra of P1 and P2 functionalised copolymers deposited on quartz by MAPLE from DMSO (Table 1) [29, 51].

As well as for monomers A5 and A6, the Raman spectra of functionalised copolymers thin films deposited by MAPLE drawn in Figure 32 show well-defined peaks in the range 200-1200 cm^{-1} being correlated with the scattering on internal vibration modes which are associated with deformation of the molecules. The peaks situated at 220 cm^{-1}, 375 cm^{-1}, 400 cm^{-1}, 480 cm^{-1} correspond to the unit 1, 2, 4-trisubstituted nucleus unit in the polymers chemical structure [51].

The band situated between 1050 and 1200 cm^{-1} could be associated with the stretching vibration of the C-C skeleton and the bands situated at low wavenumbers between 10 and 200 cm^{-1} could be correlated to external vibrations and to the relative of the MAPLE deposited thin films [51].

http://dx.doi.org/10.5772/60926

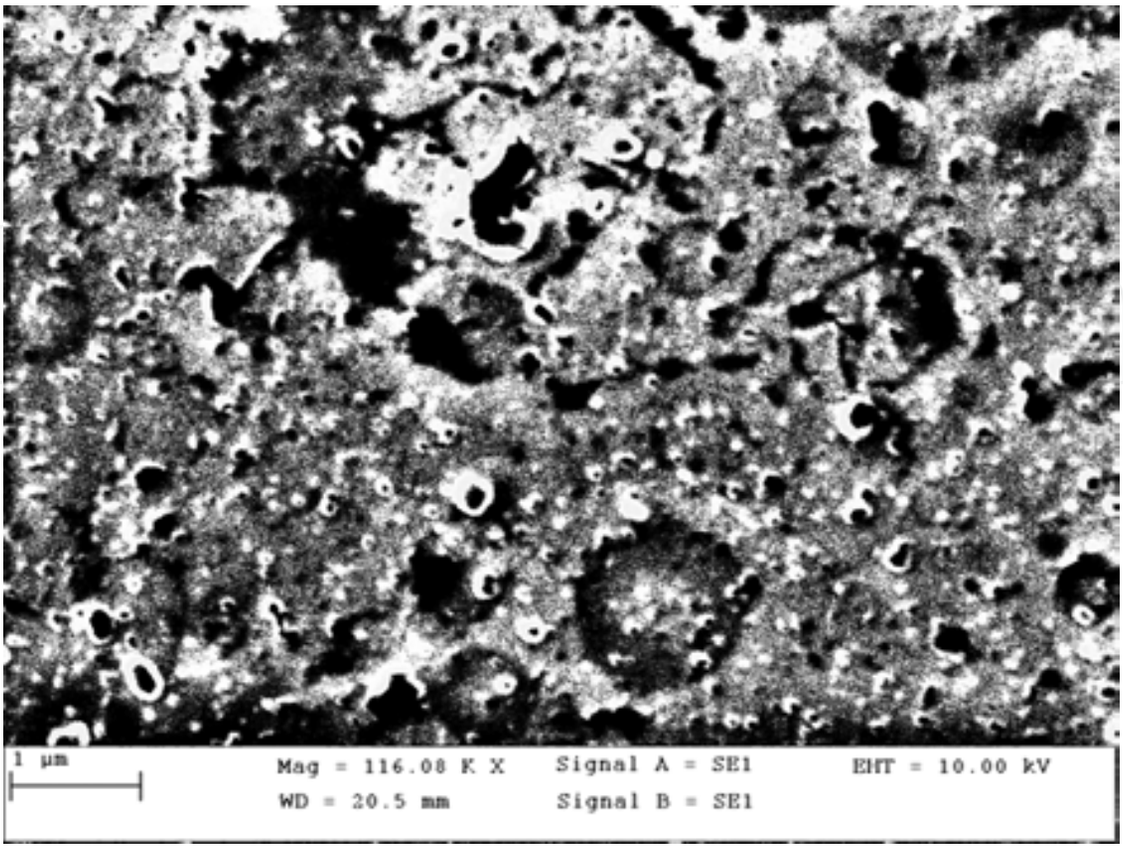

Figure 33. SEM image of P1 film deposited by MAPLE on Si from DMSO [51].

The FTIR spectra presented in Figure 29, Figure 30 and Figure 31 and Raman spectra presented in Figure 32 have not evidenced any change or damage in the chemical structure of the polymer and generation of compositional non-homogeneities in the film under the effect of laser beam.

The morphology of the MAPLE deposited P1 films evidenced by SEM in Figure 33 is relatively uniform on large area, with droplets type structures having dimension <0.1 μm [51]. During the thermal evaporation of the target, fractions of solvent matrix could be retained within the ejected matrix-polymer droplets [54].

The morphology and uniformity of the deposited films is determined by the mechanism of droplets evaporation [51]. The solvent could evaporate partially or totally during the deposition on heated substrate and this process led to the mentioned morphology [51, 54].

Different morphologies, compared to MAPLE deposited functionalised copolymers P1 and P2 thin films, have been revealed for samples of the same functionalised copolymers prepared on Si by vacuum evaporation and by spin coating in Figures 34 a and b.

A special morphology showing two types of local organisation as granules and crystals randomly oriented has been emphasised for the films deposited by vacuum evaporation. The morphology of the spin-coated films is also characterised by the presence of local organisation as granules dispersed in a uniform layer.

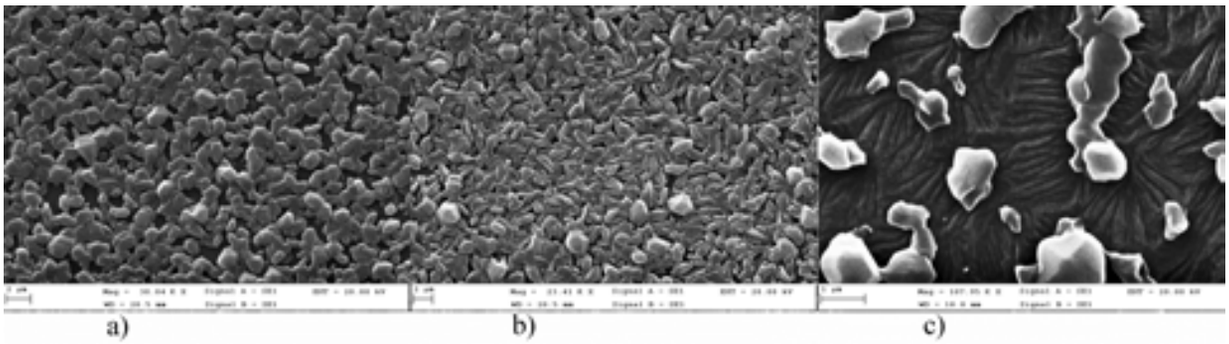

Figure 34. SEM image of: P1 deposited on Si by vacuum evaporation (a); P2 deposited on Si by vacuum evaporation (b); P1 deposited on Si by spin coating [50].

As mentioned above, the temperature involved in the vacuum deposition process can determine the fragmentation of the polymeric chain leading to entities which maintain intact the functional groups implied in the ONL phenomena. This explanation is sustained by the presence of the second, granular, phase in the vacuum evaporated films evidenced by SEM.

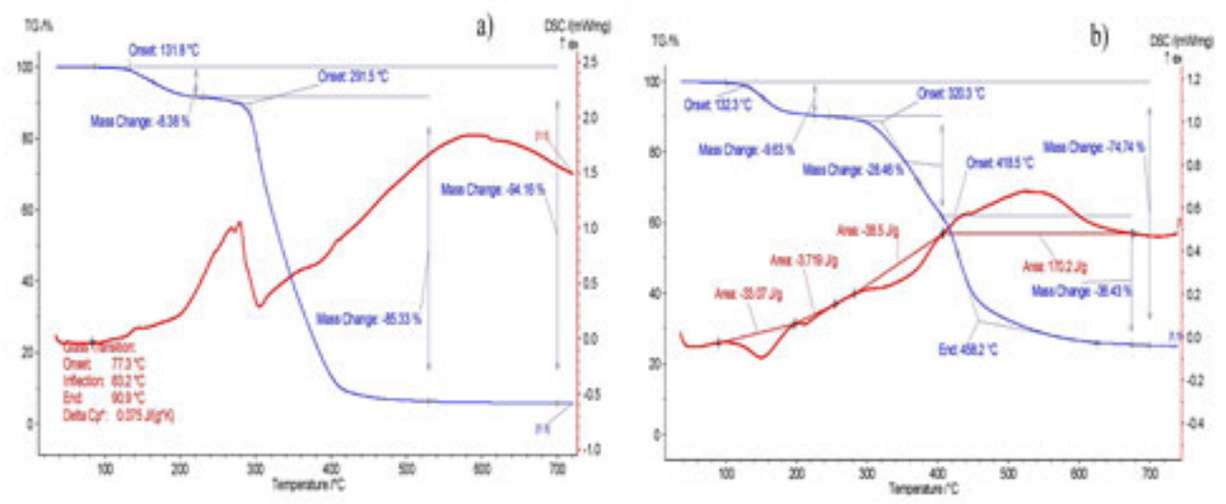

Figure 35. Thermogravimetric analysis of functionalised copolymers: P1 (a); P2 (b) [29].

The distinct crystals phase has been associated with the presence of 2, 4-dinitroaniline in excess remained ungrafted and crystallising in the films during the deposition process. The copolymer degradation process is not involved in the vacuum deposition because the temperature of 110°C is lower than the temperature of ~130°C revealed by the thermogravimetric analysis, presented in Figure 35, as the starting point for a chemical degradation of the copolymeric support. Starting with this temperature, the [-CH-CH-] groups and MA units are simultaneously lost in the both components [50].

A certain degree of short-range order in the polymeric films prepared by vacuum evaporation has been also evidenced by X-ray diffraction measurements indicated in Figure 36. This means that the fragments of the polymeric chain with anilinic moieties are ordered and the strong

http://dx.doi.org/10.5772/60926

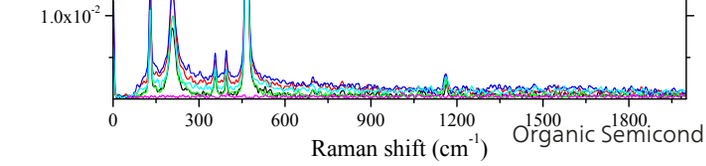

32

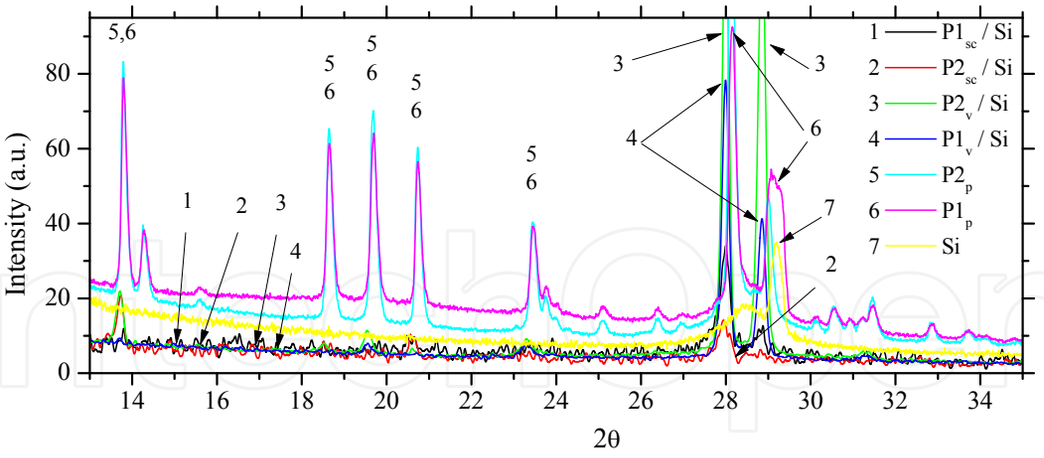

36

Figure 36. X-Ray diffractograms for films of P1 (a) and P2 (b) prepared on Si by vacuum evaporation (v) and spin coating (sc). The spectra of P1 and P2 powder (p) on Si are given as references [50].

peaks are assigned to the d_{Bragg} parameter for 2, 4-dinitroaniline [50], using the Powder Diffraction Files. The films of P1 and P2 prepared both by spin coating and vacuum evaporation have shown the same shape of the XRD spectra. The spin coating is a room temperature method and the fragmentation of the polymer chain could not be considered. The similarity between the films prepared by these two methods confirms a certain degree of order in the spin-coated layer induced by the grafted entities, the d spacing corresponding to 2, 4-dinitroaniline.

ONL phenomena evidenced in polymeric films deposited by vacuum evaporation and spin coating are presented in Figure 37a and by MAPLE in Figure 37b: the SH emission situated at 400 nm and a strong TPF emission band with a peak situated between 500 and 600 nm [50].

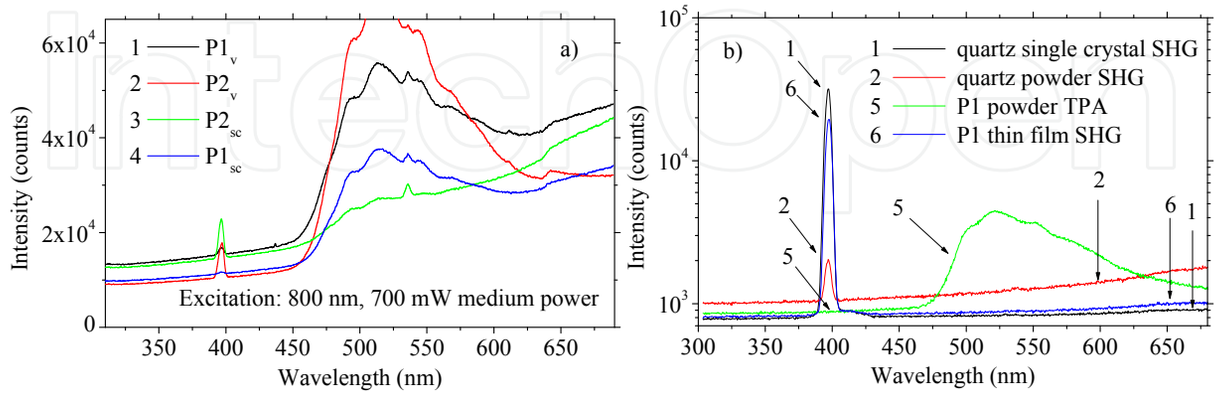

37

Figure 37. ONL effects (SHG and TPF) in functionalised copolymer P1 and P2 films prepared by vacuum evaporation (v) and spin coating (sc) (a); ONL effects (SHG and TPF) in functionalised copolymer P1 powders and thin films deposited by MAPLE (b) [50].

There is a correlation between the preparation method (vacuum evaporation, spin coating, MAPLE) of the thin films and the properties (SH and TPF emissions) of these types of maleic anhydride based copolymers functionalised with the same polar chromophoric groups bearing anilinic moieties. The SHG is obtained in these thin films showing asymmetric π electron clouds generated by the high difference in the electronegativities of the substituent groups. The ONL properties are preserved despite the potential fragmentation of the polymeric chain during the evaporation process because the potential resulting mononers/oligomers maintain intact the functional groups implied in the generation of ONL phenomena [50].

The SH measurements have been realised on thin films of P1 deposited by MAPLE on quartz and compared with that realised on powder placed on an aluminium substrate with no contribution to ONL phenomena. A broad-structured emission band situated between 500 and 600 nm was evidenced in polymer thin film and was determined by a strong luminescence emission which has been generated by a two-photon absorption process as previously mentioned [29]. As already emphasised, the functionalised copolymers prepared by MAPLE have shown SHG because of the acentric alignment of the organic molecules [43].

4. Conclusions

We summarise in this chapter some of the most significant results of our research in the field of new organic materials for optical non-linear applications. We have selected and investigated three types of organic thin films prepared from arylenevinylene compounds, maleimidic derivatives and anilinic derivatives functionalised copolymers and two types of molecular crystalline materials prepared from aromatic derivatives m-DNB and Bz.

In the context of special attention paid to the investigation of bi-component organic systems for ONL applications involving the preparation and characterisation of organic crystals and organic/organic composites, our interest was focused on studying pure and doped m-DNB and Bz bulk crystals and maleimidic derivatives monomers in polycarbonate matrix composite layers. The previous results on growth interface stability for Bz crystals have been completed with new conclusions on the stable growth of m-DNB crystals. We have emphasized the conditions favouring the initiation of instabilities, which are associated with structural defects and compositional non-homogeneities in the crystal of m-DNB affecting the optical properties including the ONL properties. New results have been bought about the systems aromatic derivative crystal/dopant studied from the point of view of the inorganic/organic dopant incorporation and its effect on the optical band gap and ONL properties of the m-DNB and Bz crystals.

The correlation between the morphology and structural order of organic/organic composite layer and the ONL properties has been discussed.

A special attention was paid to chose the adequate method for thin-films preparation, like vacuum evaporation deposition, matrix-assisted pulsed laser evaporation (MAPLE) and spin coating, in correlation with the particularities of the organic molecule: arylenevinylene (triphenylamine, carbazole) based oligomers, maleimidic derivatives monomers, aniline

derivative functionalised copolymers (maleic anhydride-vinyl benzyl chloride and maleic anhydride-methylmethacrilate supports functionalised with 2, 4-dinitroaniline).

We have analysed the correlation molecular structure-preparation conditions of the organic films determining their morphology and structure-optical non-linear (SHG and TPF) properties.

Important results have been bought in the field of maleic anhydride-based copolymers functionalised with polar chromophoric groups bearing anilinic moieties. Despite the potential fragmentation of the polymeric chain during the deposition process, the ONL properties are preserved because the potential resulting entities maintain intact the functional groups implied in the generation of these phenomena.

Further research will focus on the improvement of the organic material quality by a more rigorous control of the deposition conditions with the purpose to increase the efficiency of the ONL phenomena.

Author details

Anca Stanculescu[1*] and Florin Stanculescu[2]

*Address all correspondence to: sanca@infim.ro

1 National Institute of Materials Physics, Bucharest-Magurele, Romania

2 University of Bucharest, Bucharest-Magurele, Romania

References

[1] Freyhardt HC. ed. Crystals: Growth, Properties and Applications, Vol.4. Berlin: Springer; 1980.

[2] Babu GA, Ramasamy RP, Ramasamy P, Kumar VK. Synthesis, crystal growth, and characterization of an organic nonlinear optical donor-π-acceptor single crystal: 2-amino-5-nitropyridinium-toluenesulfonate. Crystal Growth Design 2009;9(7):3333-7.

[3] Fejer MM. Nonlinear optical conversion. Phys Today 1994;47(5):25-32.

[4] Munn RW, Miniewicz A, Kuchta B, eds. Electrical and Related Properties of Organic Solids: Dordrecht Netherlands: Kluwer Academic Publishers, 1997.

[5] Chen CP, Su Y, Jhun CG. Recent advances in holographic recording media for dynamic holographic display. J Optics Photonics 2014;1:article number 1, doi: http://dx.doi.org/10.7243/2057-1569-1-1.

[6] Agulló-López F, Cabrera JM, Agulló-Rueda F. Electrooptics. Phenomena, materials and Applications, London: Academic Press; 1994.

[7] Hillman TR, Yamauchi T, Choi W, Dasari RR, Feld MS, Park YK, Yaqoob Z. Digital optical phase conjugation for delivering two-dimensional images through turbid media. Sci Rep 2013;3:article number:1909, doi:10.1038/srep01909.

[8] Choi S-K, Vasilyev M, Kumar P. Noiseless optical amplification of images. Phys Rev Lett 1999;83(10):1938-41.

[9] Krenn M, Robert Fickler R, Fink M, Handsteiner J, Malik M, Scheidl T, Ursin R, Zeilinger A. Communication with spatially modulated light through turbulent air across Vienna. New J Phys 2014;16:113028, http://iopscience.iop.org/1367-2630/16/11/113028.

[10] Biberman A, Bergman K. Optical interconnection networks for high-performance computing systems. Rep Prog Phys 2012;75:046402, http://iopscience.iop.org/0034-4885/75/4/046402.

[11] Winter PW, Shroff H. Faster fluorescence microscopy: advances in high speed biological imaging. Curr Opin Chem Biol 2014;20:46-53.

[12] Winter PW, York AG, Nogare DD, Ingaramo M, Christensen R, Chitnis A, Patterson GH, Shroff H. Two-photon instant structured illumination microscopy improves the depth penetration of super-resolution imaging in thick scattering samples. Optica 2014;1(3):181-91.

[13] Sun H-B, Kawata S. Two-photon photopolimerization and 3D lithographic microfabrication. APS 2004;170:169-273.

[14] Goradia I, Doshi J, Deulkar KA. Review paper on 3D optical storage data. Int J Curr Eng Technol 2014;493:2933-6.

[15] Tang X-J, Wu L-Z, Zhang L-P, Tung C-H. Two-photon-pumped frequency-upconverted lasing and optical power limiting properties of vinylbenzothiazole-containing compounds in solution. Phys Chem Chem Phys 2002;4(23):5744-7.

[16] Stanculescu A, Stanculescu F. Some optical investigations on crystalline doped meta-dinitrobenzene. J Optoelectronics Adv Mater 2000;2(5):536-41.

[17] Stanculescu A, Stanculescu F, Alexandru H. Melt growth and characterization of pure and doped meta-dinitrobenzene crystals 1999;198/199(1-4):572-7.

[18] Stanculescu A, Tugulea L, Alexandru HV, Stanculescu F, Socol M. Molecular organic crystalline matrix for hybrid organic-inorganic (nano) composite materials. J Crystal Growth 2005;275(1-2):e1779-86.

[19] Stanculescu F, Ionita I, Stanculescu A. Organic/inorganic-doped aromatic derivative crystals: growth and properties. J Cryst Growth 2014;401:215-20.

[20] Stanculescu A. Investigation of the growth process of organic/inorganic doped aromatic derivatives crystals. J Optoelectronics Adv Mater 2007;9(5):1329-36.

[21] Barvinschi F, Stanculescu F, Stanculescu A. Heat transfer process during the crystallization of benzil grown by the Bridgman-Stockbarger method. J Crystal Growth 2011;317(1):23-7.

[22] Sekerka RF. Morphological stability. J Cryst Growth 1968;3(4):71-81.

[23] Mullins WW, Sekerka RF. Morphological stability of a particle growing by diffusion or heat flow. J Appl Phys 1963;34(2):323-9.

[24] Mullins WW, Sekerka RF. Stability of a planar interface during solidification of a dilute binary alloy. J Appl Phys 1964;35(2):444-51.

[25] Acree WE Jr. Thermodynamic properties of organic compounds: enthalpy of fusion and melting point temperature compilation. Thermochim Acta 1991;189(1):37-56.

[26] Urbanski T. Chemistry and technology of explosives.Vol. 3. Elsevier Sci Technol 1963:234-235.

[27] Yaws CL. Organic Compounds C5 to C7 in Handbook of Thermal Conductivity, Vol. 2, Houston: Gulf Publishing Company; 1995.

[28] Lin Y, Shi Z, Wildfong PL. Thermal conductivity measurements for small molecule organic solid materials using modulated differential scanning calorimetry (MDSC) and data corrections for sample porosity. J Pharm Biomed Anal 2010;51(4):979-84.

[29] Stanculescu A, Rasoga O, Preda N, Socol M, Stanculescu F, Ionita I, Albu A-M, Socol G. Preparation and characterization of polar aniline functionalized copolymers thin films for optical non-linear applications. Ferroelectrics 2009;389(1):159-73.

[30] Stanculescu A, Antohe S, Alexandru HV, Tugulea L, Stanculescu F, Socol M. Effect of dopant on the intrinsic properties of some multifunctional aromatic compounds films for target applications. Synthetic Metals 2004;147(1-3):215-20.

[31] Rasoga O, Vacareanu L, Grigoras M, Enculescu M, Socol M, Stanculescu F, Ionita I, Stanculescu A. Optical and electrical properties of arylenevinylene compounds thin films prepared by vacuum evaporation. Synthetic Metals 2012;161(23-24):2612-7.

[32] Grigoras M, Antonoaia NC. Synthesis of isoelectronic polyazomethine and poly(arylene vinylene) by a palladium-catalyzed Suzuki coupling method. Polym Int 2005;54(12):1641-6.

[33] Wang X, Yang P, Xu G, Jiang W, Yang T. Two-photon absorption and two-photon excited fluorescence of triphenylamine-based multibranched chromophores. Synthetic Metals 2005;155(3):464-73.

[34] Yoon KR, Ko S-O, Lee SM, Lee H. Synthesis and characterization of carbazole derived nonlinear optical dyes.Dyes Pigments 2007;75(3):567-73.

[35] Stanculescu A, Vacareanu L, Grigoras M, Socol M, Socol G, Stanculsecu F, Preda N, Matei E, Ionita I, Girtan M, Mihailescu IN. Thin films of arylenevinylene oligomers prepared by MAPLE for applications in non-linear optics. Appl Surface Sci 2011;257(12):5298-302.

[36] Mailhot-Jensen B, Robu S, Rivaton A, Pilichowski J-F, Chirita A, Chilat E, Dragalina G. Carbazole containing copolymers: synthesis, characterization, and applications in reversible holographic recording. Int J Photoenergy 2010;Article ID 945242, 11 pages. doi:10.1155/2010/945242.

[37] Leveugle E, Zhigilei LV, Sellinger A, Fitz-Gerald JM. Computational and experimental study of the cluster size distribution in MAPLE. Appl Surf Sci 2007;253(15): 6456-60.

[38] Hell SW, Booth M, Wilms S, Schnetter CM, Kirsch AK, Arndt-Jovin DJ, Jovin TM. Two-photon near- and far-field fluorescence microscopy with continuous-wave excitation. Optics Lett 1998;23(15):1238-40.

[39] Rulliere C, ed. Femtosecond Laser Pulses: Principles and experiments, N.Y.: Springer Science; 2005.

[40] Stanculescu A, Albu A-M, Socol G, Stanculescu F, Socol M, Preda N, Rasoga O, Girtan M, Iulian I. MAPLE deposited thin monomer films of maleimidic derivatives for photonics. J Optoelectronics Adv Mater 2010;12(3):731-9.

[41] Wong MS, Meier U, Pan F, Gramlich V, Bosshard C, Günter P. Five-membered hydrazone derivatives for second-order nonlinear optics. Adv Mater 1996;8(5):416-20.

[42] Chemla DS, Zyss J. Nonlinear Optical Properties of Organic Molecules and Crystals. Orlando USA: Academic Press; 1987.

[43] Kim WH, Jiang XL, Kumar J, Tripathy SK. Design of new polydiacetylenes as self assembling second order nonlinear optical polymers. Pure Appl Chem 1995;67(12): 2023-30.

[44] Lee KJ, Oh JH, Kim Y, Jang J. Fabrication of photoluminescent-dye embedded poly(methyl methacrylate) nanofibers and their fluorescence resonance energy transfer properties. Adv Mater 2006;18(17):2216-9.

[45] Rosemary MJ, Suryananayanan V, MacLaren I, Pradeep T. Aniline incorporated silica nanobubbles. J Chem Sci 2006;118(5):375-84.

[46] Bosshard Ch, Sutter K, Prêtre Ph, Hullinger J, Flörsheimer M, Kaatz P, Günter P. Organic Nonlinear Optical Materials, vol.1Switzerland: Gordon Breach Publishers; 1996.

[47] Stanculescu F, Stanculescu A, Girtan M, Socol M, Rasoga O. Effect of the morphology on the optical and electrical properties of polycarbonate film doped with aniline derivatives monomers. Synthetic Metals 2012;161(23-24):2589-97.

[48] Nalwa HS. Nonlinear Optics of Organic Molecules and Polymers. New York: CRC; 1997.

[49] Abbotto A, Beverina L, Chirico G, Facchetti A, Ferruti P, Pagani GA. Design and synthesis of new functional polymers for nonlinear optical applications. Synthetic Metals 2003;139(3):629-32.

[50] Stanculescu A, Socol M, Albu A-M, Rasoga O, Stanculescu F, Ionita I, Enculescu I. Investigation of the correlation between the preparation method and the properties of anilinic derivatives functionalised polymer thin films for non-linear optical applications. Mater Sci Forum 2010;636-7, 798-804.

[51] Socol G, Mihailescu IN, Albu A-M, Antohe S, Stanculescu F, Stanculescu A, Mihut L, Preda N, Socol M. MAPLE prepared polymeric thin films for non-linear optic applications. Appl Surface Sci 2009;255(10):5611-4.

[52] Patel CB, Malek NI, Oswals SI. Synthesis and Radical Polymerization of N-[4-N'-(Phenylamino-carbonyl)phenyl]maleimide and its Copolymerization with Methyl Methacrylate. J Macromolecular Sci Part A: Pure Appl Chem 2006; 43:289-303.

[53] Ina E, Matsumoto N, Shikada E, Kannari F. Laser ablation deposition of crystalline copper-phthalocyanine thin films. Appl Surface Sci 1998;127-129(1-2):574-8.

[54] Sellinger AT, Leveugle E, Gogick K, Peman G, Zhigilei LV, Fitz-Gerald JM. Ejection of matrix-polymer clusters in matrix-assisted laser evaporation: Experimental observation.J Phys Conf Ser 2007;59:314-7.

IntechOpen